

## Quasiparticle undressing in a dynamic Hubbard model: exact diagonalization study

J. E. Hirsch

Department of Physics, University of California, San Diego  
La Jolla, CA 92093-0319  
(March 13, 2002)

Dynamic Hubbard models have been proposed as extensions of the conventional Hubbard model to describe the orbital relaxation that occurs upon double occupancy of an atomic orbital. These models give rise to pairing of holes and superconductivity in certain parameter ranges. Here we explore the changes in carrier effective mass and quasiparticle weight and in one- and two-particle spectral functions that occur in a dynamic Hubbard model upon pairing, by exact diagonalization of small systems. It is found that pairing is associated with lowering of effective mass and increase of quasiparticle weight, manifested in transfer of spectral weight from high to low frequencies in one- and two-particle spectral functions. This ‘undressing’ phenomenology resembles observations in transport, photoemission and optical experiments in high  $T_c$  cuprates. This behavior is contrasted with that of a conventional electron-hole symmetric Holstein-like model with attractive on-site interaction, where pairing is associated with ‘dressing’ instead of ‘undressing’.

## I. INTRODUCTION

The conventional understanding of superconductivity starts from a normal state composed of weakly interacting ‘dressed’ Landau quasiparticles [1]. When the system goes superconducting these quasiparticles become correlated in Cooper pairs. As a function of increasing coupling strength, the Cooper pairs undergo a crossover from weakly bound with a long coherence length to strongly bound with a short coherence length. Because of the increased correlation of the quasiparticles in the Cooper pair their effective mass increases and their quasiparticle weight decreases compared to the normal state, the more so the stronger the coupling. In other words, the quasiparticle ‘dressing’ is larger in the superconducting than in the normal state.

Instead, the theory of hole superconductivity [2,4] proposes a new paradigm to describe superconductivity which is exactly opposite to what is described above. It also starts from a Fermi liquid of weakly interacting dressed quasiparticles, and Cooper pairs are also formed as the system goes superconducting. However, here the quasiparticles ‘undress’ and resemble more free particles when they are bound in the Cooper pair than when they are unbound in the normal state, with the effect being largest precisely in the strong coupling short coherence length regime.

This paradoxical scenario is described by a new class of model Hamiltonians recently introduced to describe correlated electrons, ‘dynamic Hubbard models’. [2,5,6] It is argued that these models capture an essential aspect of the physics of correlated electrons in atoms, molecules and solids, which is left out in other models like the conventional Hubbard model. Whether these new models describe superconductivity in any or all real materials remains to be established. The fundamental feature dis-

tinguishing these from conventional models is that they describe ‘undressing’ instead of ‘dressing’ when carriers pair. The undressing should be most apparent for superconductors with high critical temperature. In support of these models over conventional models we remark that many aspects of the phenomenology of high  $T_c$  cuprate superconductors, to be reviewed later, indicate that quasiparticles undress when they pair [7-12]. Of course there could be other unconventional models describing similar physics.

In a recent paper we have begun a numerical study of a particular realization of a dynamic Hubbard model with auxiliary spin degrees of freedom. [13] We studied the pair binding energy and lowering of kinetic energy that occurs when carriers pair as function of the parameters in the model by exact diagonalization of small clusters and quantum Monte Carlo simulations, and obtained the approximate phase diagram of the model in one dimension. The purpose of this paper is to learn more about the properties of this model by studying frequency-dependent spectral functions. The reason for doing so is that the properties of this simple model are likely to be generic for the entire class of dynamic Hubbard models and, as argued elsewhere [6], representative of the properties of correlated electrons in solids. We calculate the frequency dependent conductivity and the single particle spectral function in this model by exact diagonalization of small clusters, as well as the quasiparticle weight and effective mass, and examine their behavior as function of parameters. The results support the general scenario of ‘undressing’ in these models indicated by more approximate treatments and qualitative arguments. We contrast the behavior of this model with that of a conventional (electron-hole symmetric) model where ‘dressing’ rather than ‘undressing’ occurs upon pairing. Finally, we discuss the connection of our results to experimen-

tal observations in spectroscopic experiments in high  $T_c$  materials.

## II. MODELS

### A. Dynamical Hubbard model

The dynamical Hubbard model of interest here is defined by the Hamiltonian [6,13]

$$H = \sum_i H_i - t \sum_{\langle i,j \rangle} [c_{i+1}^\dagger c_i + \text{h.c.}] \quad (1)$$

where the local Hamiltonian  $H_i$  in electron representation is

$$H_i = \epsilon_0 \frac{\sigma_x}{2} + g \frac{\sigma_z}{2} + [U - 2g] \frac{\sigma_z}{2} n_{i\uparrow} n_{i\downarrow} \quad (2a)$$

and in hole representation

$$H_i = \epsilon_0 \frac{\sigma_x}{2} + g \frac{\sigma_z}{2} [2(n_{i\uparrow} + n_{i\downarrow}) - 1] \frac{\sigma_z}{2} + [U - 2g] \frac{\sigma_z}{2} n_{i\uparrow} n_{i\downarrow} \quad (2b)$$

and  $\frac{\sigma_x}{2}, \frac{\sigma_z}{2}$  are Pauli matrices associated with an auxiliary spin-1/2 degree of freedom at each site. In what follows the Hamiltonian in hole representation will be used.  $U$  is the effective on-site interaction. Briefly, the auxiliary spin is introduced to allow for the fact that two electrons on a site can be in more than one state: depending on the orientation of the auxiliary spin, they will experience more or less Coulomb repulsion and in turn pay less or more in kinetic and single-electron potential energy, described by the energy of the auxiliary spin. A more detailed justification of the site Hamiltonian Eq. (2) to describe the physics of real atoms is discussed in ref. [13].

In the antiadiabatic limit  $\epsilon_0 \rightarrow 1$  the effective low energy Hamiltonian for low hole concentration is [13]

$$H_{\text{eff}} = \sum_{\langle i,j \rangle} [t_2 + t(n_{i\uparrow} + n_{i\downarrow})] (c_{i+1}^\dagger c_i + \text{h.c.}) + U \sum_i n_{i\uparrow} n_{i\downarrow} \quad (3a)$$

$$t_2 = S^2 t \quad (3b)$$

$$t = tS(1 - S) \quad (3c)$$

$$S = \frac{1}{1 + g^2} \quad (3d)$$

which describes ground-state to ground-state transitions of the spin degree of freedom at each site when the holes hop. This Hamiltonian gives rise to pairing of two holes in a full band if the condition

$$\frac{U}{4t} < \frac{g^2}{1 + g^2} \quad (4)$$

is satisfied. As shown in Ref [13], the condition for pairing for finite  $\epsilon_0$  is considerably less stringent than Eq. (4).

### B. Electron-hole symmetric Holstein-like model

Conventional electron-boson models involve coupling of a boson (e.g. phonon) degree of freedom to the electronic charge density, and are electron-hole symmetric. We will contrast the behavior of the dynamical Hubbard model with that of a model with site Hamiltonian

$$H_i = \epsilon_0 \frac{\sigma_x}{2} + g \frac{\sigma_z}{2} [n_{i\uparrow} + n_{i\downarrow} - 1] + U_0 n_{i\uparrow} n_{i\downarrow} \quad (5)$$

as a generic 'conventional' model. Some properties of this Hamiltonian were discussed in ref. [13]. The effective on-site interaction is

$$U = U_0 - 2\epsilon_0 \left( \frac{1}{1 + g^2} - 1 \right) \quad (6)$$

The low energy effective Hamiltonian in the antiadiabatic limit with  $\epsilon_0 \rightarrow 1$ ,  $g$  fixed and  $U$  fixed (i.e.  $U_0 \rightarrow 1$  also) is

$$H_{\text{eff}} = t_{\text{eff}} \sum_{\langle i,j \rangle} (c_{i+1}^\dagger c_i + \text{h.c.}) + U \sum_i n_{i\uparrow} n_{i\downarrow} \quad (7a)$$

with

$$t_{\text{eff}} = tS^2 \quad (7b)$$

$$S = \langle 0 | j | \rangle = \langle 1 | j | \rangle = \frac{S}{2} \frac{1}{(1 + \frac{1}{1 + g^2})} \quad (7c)$$

and it gives rise to pairing only if  $U < 0$  (attractive Hubbard model). For finite  $\epsilon_0$  we find that the condition for pairing is even more stringent than  $U < 0$ . In contrast to the dynamical Hubbard model, here  $S$  does not become small as  $g \rightarrow 1$ .

## III. SPECTRAL FUNCTIONS

### A. Optical conductivity

We will compute the optical conductivity in these models at zero temperature, given by

$$\chi_1(\omega) = \sum_m \frac{\langle j | \langle 0 | j | n \rangle \rangle^2}{E_m - E_0} \delta(\omega - (E_m - E_0)) \quad (8)$$

with the current operator given by

$$J = it \sum_i [c_{i+1}^\dagger c_i - c_i^\dagger c_{i+1}] \quad (9)$$

It is easily shown following the steps in Madaque's derivation [14] that the sum rule

$$\sum_0^\infty \omega \chi_1(\omega) = \frac{1}{2} \langle 0 | [J, J] | 0 \rangle \quad (10)$$

holds for these models, with  $T$  the bare kinetic energy operator

$$T = \sum_{i,j} t_{ij} [c_i^\dagger c_{j+1} + \text{h.c.}] \quad (11)$$

When the frequency  $\omega_0$  is not very small there is a natural separation of energy scales in the Hamiltonians. A low-lying submanifold of states in the Hilbert space corresponds to states where each site spin is at its site ground state, which is different depending on the electronic occupation [13]. The effective Hamiltonian Eq. (3) or Eq. (7) describes the coupling between those low-lying states, where the electrons hop from site to site and the spins make ground-state to ground-state (diagonal) transitions. This part of the Hilbert space corresponds to the quasiparticle band, and the optical absorption involving transitions between those states is the low frequency 'intra-band' part of  $\chi_1$ , corresponding to the Drude part of the optical conductivity. We can then decompose the integral of the optical conductivity as

$$\int_0^{\omega_1} d\omega \chi_1(\omega) = \int_0^{\omega_m} d\omega \chi_1(\omega) + \int_{\omega_m}^{\omega_1} d\omega \chi_1(\omega) = A_1 + A_h \quad (12)$$

where  $A_1$  is the intra-band absorption and  $\omega_m$  is a frequency cutoff that restricts optical transitions to the subset of intra-band states. On the other hand, an optical sum rule also holds for the effective Hamiltonians

$$\int_0^{\omega_1} d\omega \chi_1^{\text{eff}}(\omega) = \frac{1}{2} \langle 0 | T_{\text{eff}} | 0 \rangle \quad (13)$$

where

$$T_{\text{eff}} = \sum_{i,j} [t_{ij} + t(n_{i\downarrow} + n_{i+1\downarrow})] [c_i^\dagger c_{j+1} + \text{h.c.}] \quad (14)$$

for the site Hamiltonian Eq. (2) and

$$T_{\text{eff}} = \sum_{i,j} t_{\text{eff}} [c_i^\dagger c_{j+1} + \text{h.c.}] \quad (15)$$

for the site Hamiltonian Eq. (5), and where  $\chi_1^{\text{eff}}$  is computed from Eq. (8) with the eigenstates and eigenvalues of the effective Hamiltonians. Because the low-lying spectrum and eigenstates of the full Hamiltonians coincide with those of the effective Hamiltonians we can write Eq. (13) as a 'partial' conductivity sum rule for the low-lying eigenstates and eigenvalues of the full Hamiltonian

$$\int_0^{\omega_m} d\omega \chi_1(\omega) = A_1 = \frac{1}{2} \langle 0 | T_{\text{eff}} | 0 \rangle \quad (16)$$

The ground state  $|0\rangle$  on the right side of Eq. (16) is the ground state of the effective Hamiltonian Eq. (3) or Eq. (7).

For the effective Hamiltonian of the dynamical Hubbard model Eq. (3) it can be seen within BCS theory [15], as well as from the exact solution in the dilute limit [16] that when pairing occurs the right-hand side of Eq. (16) increases. This extra spectral weight signals a lowering of kinetic energy and effective mass reduction in the quasiparticle band. In a real physical system the total integrated optical spectral weight is conserved, so that any extra spectral weight at low frequency has to come at the expense of spectral weight in another frequency range. In tight binding models however the total optical spectral weight is not conserved, because the current and kinetic energy operators do not describe transitions to states in other bands. As a consequence, the total integral Eq. (12) does not remain constant but also increases upon pairing in our model. Nevertheless, we will see in the numerical results that the dominant effect of pairing in the dynamical Hubbard model is a large increase in the low frequency 'intra-band' spectral weight  $A_1$  and an overall shift in optical spectral weight from higher to lower frequencies.

In contrast, we will see that in the electron-hole symmetric model, the behavior is exactly opposite: in the paired state the effective mass of the carriers increases hence optical spectral weight is transferred from the quasiparticle band to higher frequencies.

## B. One-particle spectral function

The changes in the optical conductivity upon pairing are intimately related to changes in the one-particle spectral functions. We consider here the spectral function for hole destruction in a system of  $n+1$  holes, defined as [6]

$$A_{n+1,m}(\omega) = \sum_{j < j_n} \langle j | j_n j_k j_{n+1} | j \rangle (\epsilon_1^n - \epsilon_0^n) \quad (17a)$$

as well as the spectral function for hole creation in a system of  $n$  holes:

$$A_{n,m+1}(\omega) = \sum_{j < j_{n+1}} \langle j | j_{n+1} j_k j_n | j \rangle (\epsilon_1^{n+1} - \epsilon_0^n) \quad (17b)$$

Here,  $|j_n\rangle$  denotes the  $j_n$ th excited state of the system with  $n$  holes. In the exact diagonalization calculation we will study clusters with one hole and two holes of opposite spin. The relevant momentum is then  $k = 0$ .

Consider these functions for a single site in the dynamical Hubbard model. They are given by

$$A_{21}(\omega) = A_{12}(\omega) = \chi(\omega) \quad (18a)$$

$$A_{10}(\omega) = A_{01}(\omega) = S^2(\omega) + (1 - S^2)(\omega - 2\epsilon_0) \frac{P}{1 + g^2} \quad (18b)$$

with  $S$  given by Eq. (3d). The  $\omega = 0$  part corresponds to the quasiparticle contribution, and its coefficient is the quasiparticle weight  $z$ . It can be seen that for the single site,  $z = 1$  for the spectral function involving one and two holes and  $z < 1$  for the spectral function involving zero and one hole. In an extended system, when  $z < 1$  there will be an 'incoherent' contribution to the spectral function represented in the site by the second term in Eq. (18b). Hence we expect in an extended system that in the unpaired state the quasiparticle weight will be small, and that when pairing occurs spectral weight in the single particle spectral function will be transferred from the high frequency incoherent part to the  $\omega = 0$  quasiparticle peak. Correspondingly, optical transitions involving transitions between singly and doubly occupied sites will have larger low energy spectral weight than those involving empty and singly occupied sites, and optical spectral weight should be transferred from high frequencies to low frequencies when pairing occurs.

In contrast, in the electron-hole symmetric model the spectral functions for creation of a hole in a singly occupied site and destruction of a hole in a singly occupied site are both given by

$$A_{12}(\omega) = A_{10}(\omega) = S^2(\omega) + (1 - S^2)(\omega - 2\epsilon_0) \frac{p}{1 + g^2} \quad (19a)$$

and the spectral functions for destruction of a hole in a doubly occupied site and creation of a hole in an empty site are given by

$$A_{21}(\omega) = A_{01}(\omega) = S^2(\omega) + (1 - S^2)(\omega - 2\epsilon_0) \quad (19b)$$

where  $S$  is given by Eq. (7c). It can be seen that the quasiparticle weight is the same for all these spectral functions ( $z = S^2$ ), whether the site is initially empty, singly or doubly occupied. Hence we cannot extract any conclusions about changes in the quasiparticle weight upon pairing from 'single site' physics in this model. In an extended system however because of the more correlated nature of the wavefunction in the paired state we will see that pairing is associated with decrease of the quasiparticle weight, i.e. increased 'dressing', in contrast to the behavior in the dynamical Hubbard model. Similarly one would expect transfer of optical spectral weight from low frequencies to high frequencies upon pairing in this model, in contrast to the behavior in the dynamical Hubbard model.

#### IV. NUMERICAL RESULTS

We diagonalize exactly the Hamiltonian Eq. (1) with site Hamiltonians Eq. (2b) (dynamical Hubbard model) and Eq. (6) (electron-hole symmetric model) for four sites in the subspaces with zero-, one- and two-hole occupation. We choose units so that  $t = 1$ . For a finite chain, the optical sum rule Eq. (10) holds if free ends

boundary conditions are used, but not if periodic boundary conditions are used; in the latter case, an extra term proportional to a zero-frequency  $\delta$ -function is needed to satisfy the sum rule [17]. We will use free ends boundary conditions to calculate the optical conductivity, so that the total optical spectral weight is obtained in the numerical calculation. The lowest frequency peak then occurs at a finite frequency  $\omega_D$  ('D' stands for 'precursor') [17] that goes to zero as the size of the system increases.

#### A. Dynamical Hubbard model

To obtain a clear separation of energy scales that illustrates clearly the physics of the model we choose a strong coupling case, with  $g = 3$ . The single hole effective hopping Eq. (3b) in the adiabatic limit is then  $t_2 = 0.1$ , and  $t = 0.216$ . The site energies for  $n$  holes (excluding the  $U$  term) are given by

$$\epsilon(n) = \epsilon(0) + \frac{p}{1 + g^2} \quad (20)$$

with  $\epsilon(n)$ ;  $\epsilon(0)$  the energies of the site ground state and excited state. Hence the difference  $\epsilon(n) - \epsilon(0) = 6.3\epsilon_0$  is much larger than the effective bandwidth for the holes except for very small  $\epsilon_0$ . Even so, for the case of 2 holes the effective Hamiltonian Eq. (3) is not an accurate representation for finite frequencies because of the contributions from 'vertical transitions' as discussed in ref. [13]; the effective interaction

$$U_{\text{eff}} = E(2) + E(0) - 2E(1) \quad (21)$$

( $E(n)$  = energy with  $n$  holes) is considerably more attractive for finite frequency than in the adiabatic limit  $\epsilon_0 \rightarrow 1$  where the effective Hamiltonian Eq. (3) is valid. We will use  $\epsilon_0 = 1$  here.

Figure 1 shows the effective interaction versus the on-site repulsion  $U$ . For  $\epsilon_0 = 1$  it is attractive for  $U < 5.9$ , while in the adiabatic limit it is attractive only for  $U < 3.6$ .

It is interesting to consider the structure of energy levels, shown in Figure 2. We show the energy levels for a single hole in the system and for two holes in the cases  $U = 8$  and  $U = 0$ . The effective interaction for these two cases is  $U_{\text{eff}} = 0.056$  and  $U_{\text{eff}} = 0.715$  respectively. There is a clear separation between low-lying energy levels, described by an effective 'intra-band' Hamiltonian and higher-lying levels where the spin degrees of freedom are in excited states. In the single particle case there are 4 low-lying states, in the two-particle case there are 16 low-lying states for  $U = 0$ , for  $U = 8$  there are only 12 because 4 'intra-band' states are pushed high in energy due to the strong on-site repulsion. Note also that the energy range of the low-lying states is considerably larger for the case  $U = 0$  than for  $U = 8$ . This reflects the bandwidth expansion that occurs upon pairing in this model.

Figure 3 shows the frequency-dependent conductivity for on-site repulsion  $U = 8$  (solid line) and for  $U = 0$  (dashed line). For  $U = 8$  the holes are not bound since  $U_{eff} > 0$ , while for  $U = 0$  the holes are bound with  $U_{eff} = 0.715$ . The low frequency 'intraband' conductivity is seen to increase substantially when the holes are paired. Furthermore, the optical absorption at intermediate frequencies ( $\omega_0 \approx 6$ ) increases upon pairing, while the optical absorption at the highest frequencies ( $\omega > 10$ ) decreases upon pairing. This shows that optical spectral weight is transferred from high to low frequencies when pairing occurs. Interestingly, not only the 'intraband' optical spectral weight increases but also spectral weight at intermediate frequencies. This will be discussed further in the next section. Note that changes in optical spectral weight occur at energies much higher than the scale of the pairing energy,  $|J_{eff}| \approx 0.7$ .

In Figure 4a we show the optical spectral weight associated with the intra-band optical transitions  $A_1$  as well as the total optical spectral weight  $A_1 + A_h$  versus on-site repulsion  $U$ . As mentioned earlier the model does not conserve total optical spectral weight, hence  $A_1 + A_h$  is not a constant; nevertheless, the intraband spectral weight increases faster than the total spectral weight as pairing occurs, and the ratio  $A_1/A_h$  increases as  $U$  decreases as shown in Figure 4b. Hence the model does describe a transfer of optical spectral weight from high frequencies to low frequencies as pairing occurs.

Figure 4a also shows the optical spectral weight in the antiadiabatic limit  $\omega_0 \rightarrow 1$ . As  $\omega_0$  increases the high frequency optical spectral weight moves to higher frequencies and decreases in amplitude, and vanishes for  $\omega_0 = 1$ . However the low frequency  $\omega_1(\omega)$  shows very little dependence on  $\omega_0$  and its total weight is almost the same for  $\omega_0 = 1$  and  $\omega_0 = 1$  as seen in Figure 4a.

The 'undressing' process that occurs upon pairing is also clearly seen in the one-particle spectral functions. Figure 5 shows the spectral functions for single hole destruction in the system with one hole,  $A_{10}(\omega)$ , and in the system with two holes,  $A_{21}(\omega)$ . The lowest frequency peaks are actually  $\delta$ -functions at zero energy, their weight is the quasiparticle weight. For the system with a single hole, the quasiparticle weight is  $z = 0.174$ . This is larger than the quasiparticle weight for a single site for these parameters ( $z = 0.1$ ); in the extended system, finite  $\omega_0$  gives rise to a larger quasiparticle weight due to retardation. The quasiparticle weight for the two-hole system and large on-site  $U$  is very similar to the single hole spectral weight,  $z = 0.176$ . When  $U$  decreases and a pair is formed, the quasiparticle weight increases, to  $z = 0.422$  when  $U = 0$ . As seen in Figure 5b, spectral weight is transferred from the incoherent region of the spectral function at energies around  $\omega \approx 6$  to the quasiparticle peak. This energy range corresponds to states where one of the background spins in the system is in a  $\beta$  excited state. There is also a very small but finite spectral weight in the energy region around  $\omega \approx 12$ , where two of the background spins are in excited states

in the  $\beta$  excited state.

Figure 6 shows the spectral function for hole creation in a system of zero and one hole,  $A_{01}(\omega)$  and  $A_{12}(\omega)$ . Unlike the spectral functions for hole destruction they satisfy the sum rule

$$\sum_{\omega=0}^{\infty} \omega A_{n,n+1}(\omega) = 1 \quad (22)$$

( $n = 0$  or  $1$ ) because they have no negative frequency component. The quasiparticle weights extracted from these spectral functions are of course the same as those obtained from Figure 5. It is interesting to note that in the intra-band energy range ( $\omega < 2$ ) there is now an incoherent contribution to the spectral function  $A_{12}(\omega)$  for parameters where the effective interaction is attractive. The 'intraband' part of the ground state pair wavefunction is of the form

$$|j\rangle = \sum_k f(k) c_{k\uparrow}^\dagger c_{k\downarrow}^\dagger |j\rangle \quad (23)$$

and it has finite overlap with states other than  $c_{0\uparrow}^\dagger c_{0\downarrow}^\dagger |j\rangle$ . Still the weight of the coherent part of the spectral function, i.e. the zero frequency peak (quasiparticle weight) increases strongly as the pair is formed.

The behavior of quasiparticle weights as function of on-site repulsion is shown in Figure 7. For large repulsive  $U$ , the quasiparticle weight for a hole is the same for the system with two holes (dashed line) and with one hole (full line); as the on-site repulsion decreases and the pair forms, the quasiparticle weight in the system with two holes increases, indicating that 'undressing' occurs. We also show the corresponding results in the  $\omega_0 = 1$  limit, which show similar behavior; the quasiparticle weights in this case are smaller than for finite frequency. For the single hole, the quasiparticle weight in the antiadiabatic limit is the same as for the single site,  $z = S^2$ .

In summary, these results show that in the dynamic Hubbard model there is 'undressing' when pairing occurs: spectral weight in both one- and two-particle spectral functions is transferred from high to low frequencies, the quasiparticle weight increases and the kinetic energy decreases when pairing occurs. We next discuss the situation for the electron-hole symmetric model.

#### B. Electron-hole symmetric Holstein-like model

We consider the electron-hole symmetric (e-h sym) model Eq. (5), for parameters  $g = 3$  and  $\omega_0 = 1$ . The site energies for  $n$  holes in this case are

$$\epsilon_n = \epsilon_0 + \frac{P}{1 + g^2} \quad (24a)$$

for  $n = 0$  and  $n = 2$ , and

$$\epsilon_n = \epsilon_0 \quad (24b)$$

for  $n = 1$ . Because the excitation energy of the background spin is lower for the singly occupied site here there is not such a clear separation of energy scales for this model as for the dynamical Hubbard model for the parameters used.

Figure 8 shows the effective interaction between two holes in the four-site cluster versus on-site repulsion, as well as the results in the antiadiabatic limit  $t_0 = 1$ . Note that retardation is detrimental to pairing in this model. For  $t_0 = 1$ , the effective interaction is attractive for on-site repulsion  $U$  smaller than  $0.4$ .

The optical conductivity for two holes in the cluster is shown in Figure 9, for on-site repulsion  $U = 2$ , where the effective interaction is repulsive, and for  $U = -2$  where it is attractive. In this case a transfer of optical spectral weight from low to high frequencies occurs upon pairing, opposite to the behavior in the dynamical Hubbard model seen in Figure 3. Note also that the separation between low and high energy regions is less clear here than in the previous case, as expected.

The dependence of optical spectral weights on the on-site repulsion is shown in Figure 10a. The intra-band spectral weight decreases by a factor of 2 as pairs form; this indicates that the carriers are more heavily dressed and have larger effective mass in the paired state, as one would expect; in the  $t_0 = 1$  limit this model becomes equivalent to an attractive Hubbard model, where the pair mobility is always smaller than the single particle mobility [18]; in particular in the strong coupling limit the pair hopping is  $t_p = 2t^2/J$  much smaller than the single particle hopping for large on-site attraction. This model then describes a transfer of optical spectral weight from low to high frequencies when pairing occurs; the ratio of intra-band to inter-band optical spectral weights versus on-site  $U$  is shown in Fig. 10b, qualitatively different from the corresponding results for the dynamical Hubbard model Figure 4b.

The single particle spectral functions for hole destruction are shown in Figure 11. The quasiparticle weight for the system with a single hole is  $z = 0.89$ , for the system with two holes it is  $z = 0.79$  for the case  $U = 2$  with unpaired holes, and it decreases to  $z = 0.64$  for  $U = -2$  when the holes are paired. Note that this is not a single-site effect, as for a single site the spectral weight for one and two holes is identical due to electron-hole symmetry (Eq. (19)). Figure 11b shows that spectral weight from the quasiparticle peak is transferred to higher frequencies around  $\omega = 3$  when pairs form. Similarly, Figure 12 shows the single particle spectral function for hole creation in the system with zero and with one hole. For the creation of a hole in the empty cluster the incoherent part is here at lower frequencies due to the lower excitation energy of the singly-occupied site, Eq. (24b). Again, Figure 12b shows that as pairing occurs spectral weight is transferred from the quasiparticle peak to higher frequencies.

Figure 13 shows the variation of quasiparticle weight versus on-site repulsion in this model. Because for the

single site the quasiparticle weight is independent of hole occupation the variation here is less than in the dynamical Hubbard model (Figure 7). The quasiparticle weight in the system with 2 holes decreases as the pair formed, indicating that the quasiparticle is more heavily dressed in the paired compared to the unpaired state, qualitatively different to the situation in the dynamical Hubbard model.

Figure 13 also shows the quasiparticle weights in this model in the antiadiabatic limit, where it is equivalent to the Hubbard model. Note that the quasiparticle weights for the system with 1 and 2 holes coincide for  $U = 0$ , where the Hamiltonian describes non-interacting holes, and are both given by the site value  $z = S^2 = 0.658$ ; both for repulsive and attractive  $U$  the quasiparticle weight is smaller in the two-hole system due to 'intra-band' hole-hole interaction. The suppression of quasiparticle weight however is larger for negative than for positive  $U$ .

### C. Summary

The qualitatively different behavior of the two models considered is summarized in Figure 14. We plot the effective mass enhancement and the quasiparticle weight as function of the effective interaction  $U_{eff}$  in both models. The ratio of effective masses for the single particle and the pair,  $m_s/m_p$ , is obtained from the ratio of the intra-band optical spectral weight for the system with two holes and twice the intra-band optical spectral weight for the system with one hole. Figure 14a shows that in the dynamical Hubbard model the pair becomes increasingly lighter than the single particle as the interaction becomes more attractive, while in the electron-hole symmetric model the pair becomes increasingly heavier as the interaction becomes more attractive. Similarly, the quasiparticle weight increases in the dynamical Hubbard model as the pair is formed, while it decreases in the electron-hole symmetric model. In summary, the system becomes more coherent in the paired state in the dynamical Hubbard model and more incoherent in the electron-hole symmetric model.

It is interesting to note that the quasiparticle weight and the effective mass change by approximately the same factor in the dynamical Hubbard model in the parameter range considered, 2.5 and 2.4 respectively. This is what one would expect if the physics of the model is dominated by 'single site' physics, where the quasiparticle weight and effective hopping and hence effective mass are both determined by the single site overlap matrix element  $S$ . More generally, in a many body system the exact single particle Green's function is given by [19]

$$G(k; \omega) = \frac{1}{\omega - \epsilon_k - \Sigma(k; \omega)} = \frac{Z_k}{\omega - \tilde{\epsilon}_k} + G^0(k; \omega) \quad (25)$$

with  $\Sigma(k; \omega)$  the self-energy,  $\tilde{\epsilon}_k$  the quasiparticle energy and  $G^0$  the incoherent part of the Green's function. The

quasiparticle weight  $z_k$  and effective mass enhancement are given by

$$z_k = (1 - \frac{\partial}{\partial \epsilon} \text{Re}(\Sigma(k; i))^{-1} \quad (26a)$$

$$\frac{m}{m_0} = \frac{\partial \epsilon_k}{\partial k} = z_k (1 + \frac{\partial \text{Re}(\Sigma(k; i))}{\partial \epsilon_k}) \quad (26b)$$

( $\text{Re} =$  real part of  $\Sigma$ ) so that if the self-energy is momentum independent the quasiparticle weight and effective mass renormalization coincide. Hence our results indicate that this is approximately the situation in the dynamic Hubbard model, and suggest that dynamical mean field theory [20], which assumes a momentum-independent self-energy, should be a useful approach to study these models. In contrast, the results for the electron-hole symmetric model in the parameter range considered yield an effective mass changing by a factor 1.9 with the quasiparticle weight changing by a factor of only 1.2, suggesting that for this model the momentum-dependence of the self-energy is substantial.

#### D. Finite temperatures

We have also studied the behavior of the optical conductivity in the dynamic Hubbard model at finite temperatures, given by

$$\chi_1(\omega) = \frac{X}{Z} \sum_{n,m} \frac{e^{-E_n} - e^{-E_m}}{E_m - E_n} \langle 0 | j | n \rangle \langle n | j | m \rangle \quad (27)$$

with  $Z = \sum_n e^{-E_n}$  the partition function. Figure 15 shows  $\chi_1(\omega)$  for a case where the effective interaction is attractive,  $U_{\text{eff}} = 0.715$ . The intra-band part of the optical absorption is rapidly suppressed as the temperature increases, and the peak at intermediate frequencies is also suppressed. Unfortunately because tight binding models do not satisfy the optical sum rule the total optical spectral weight in the model is not conserved as the temperature changes. Nevertheless it is interesting to note that as  $T$  increases optical spectral weight is transferred to the very high frequency region  $\omega > 10$ . This change in high frequency spectral weight occurs on a temperature scale ( $T = 1$ ) that is related to the energy scale of the pairing energy ( $U_{\text{eff}}$ ) and unrelated to the energy scale of the frequency where the optical absorption change occurs.

#### V. RELATION WITH EXPERIMENTS

The dynamic Hubbard model describes a coupling of electrons to a background degree of freedom (the auxiliary spin) that only exists when the site is doubly occu-

ried by electrons. Hence its effect decreases with increasing local hole concentration, on the average the coupling constant is

$$g(n) = g_0 (2 - n) \quad (28)$$

with  $n$  the average hole concentration per site. This leads to a phenomenology whereby hole carriers ‘undress’ in the presence of other hole carriers. The undressing manifests itself in transfer of optical spectral weight from high to low frequencies and in transfer of one-particle spectral weight from the incoherent (high frequency) to the coherent (low frequency) region; these spectral weight transfers lead to increase in the quasiparticle weight and decrease in the quasiparticle effective mass. Because a hole comes close to another hole both when the hole concentration is increased by doping in the normal state as well as when carriers pair, undressing will occur both for increasing carrier concentration and for decreasing temperature.

There is substantial evidence for such phenomenology in the high  $T_c$  cuprates. Johnson et al [9] extract from photoemission experiments in the normal state a coupling constant that decreases continuously as the hole doping increases, as well as a mass enhancement that decreases with hole doping. In the overdoped regime, Yusof et al [21] find evidence from photoemission for the existence of quasiparticles in the normal state, which appear to be absent in the underdoped regime. This is consistent with the phenomenology of the dynamic Hubbard model in a strong coupling regime where the quasiparticle weight for low hole density would be small enough to be unobservable. The quasiparticle weight in the dynamic Hubbard model as a function of hole concentration is approximately given by

$$z(n) = S^2 (1 + \frac{n}{2})^2 \quad (29a)$$

$$= \frac{1}{S} - 1 \quad (29b)$$

If the coupling strength  $g$  is large  $S$  will be small,  $z$  becomes very small in the underdoped regime, and at the same time the ‘undressing parameter’ becomes large, hence quasiparticles undress rapidly with increasing  $n$ .

Ando et al [8] extract from transport measurements a hole mobility that increases monotonically with hole doping, consistent with the behavior predicted by the dynamic Hubbard model and its low energy effective Hamiltonian Eq. (3), which leads to an effective density-dependent hole hopping

$$t_{\text{eff}}(n) = t_2 + n t \quad (30)$$

which is equivalent for low  $n$  to the more fundamental relation

$$t_{\text{eff}}(n) = t z(n) \quad (31)$$

describing the fact that the quasiparticle effective mass is inversely proportional to the quasiparticle weight as expressed by Eq. (26b) when the self-energy has no momentum dependence.

Ding et al [7] make a compelling description of the undressing phenomenology of high  $T_c$  cuprates: from their photoemission data they extract a quasiparticle weight that emerges from an incoherent background as the temperature is lowered and the system becomes superconducting. This is of course consistent with the phenomenology of the dynamical Hubbard model in the strong coupling regime where  $z$  will increase strongly when pairing occurs, as seen in Figs. 5 and 7. Furthermore Ding et al find that  $z$  increases as the doping increases, again consistent with the behavior expected in the dynamical Hubbard model.

In the finite cluster calculations reported here for the optical conductivity we cannot distinguish whether the optical spectral weight transferred to low frequencies when pairing occurs goes into the zero-frequency function or to finite frequencies. However the effective Hamiltonian for the dynamical Hubbard model clearly describes transfer of spectral weight to the function as the pairing amplitude develops [15,16], since the average effective kinetic energy

$$T_{\text{eff}} = \sum_i \langle t_{\text{eff}}(i) \rangle = \langle c_i^\dagger c_{i+1} + h.c. \rangle \quad (32)$$

$$2 t \langle c_i^\dagger c_i^\dagger c_i^\dagger c_i^\dagger \rangle = \langle c_i^\dagger c_{i+1} \rangle + h.c.]$$

has a contribution from anomalous expectation values, while the intra-band optical absorption is unchanged except for the depletion due to the opening of the superconducting energy gap [22]. This indicates that the optical spectral weight transferred into the intra-band region goes into the zero-frequency function, and will lead to an apparent violation of the Ferrell-Glover-Tinkham optical sum rule [15]. This violation has been observed experimentally, both for in-plane as well as c-axis light polarization by Santander-Cyro et al [11] and by Basov et al [10] respectively. The decrease in high frequency spectral weight predicted by the dynamical Hubbard model (range above  $\omega \approx 10$  in Figs. 3 and 15) is also consistent with recent experimental observations by Molegraaf et al [12], who report a decrease in optical spectral weight in the energy range between 1.25 eV and 2.5 eV which is transferred to lower frequencies. This is also consistent with earlier observations by Fugolet al [23].

Note that our results for the dynamical Hubbard model predict also an increase in optical spectral weight at intermediate frequencies,  $\omega \approx 6$  when the interaction becomes attractive (Fig. 3) or when the temperature decreases (Fig. 15), well above the 'intra-band' frequency range. We expect this to be a generic feature of these models, describing optical transitions where a hole is transferred to a nearest neighbor site already occupied by another hole, leaving the auxiliary spin behind in an excited state. Such a 'vertical' transition will have a large weight in the

paired state (proportional to 1 rather than to  $S$  if the neighboring site is unoccupied) and enhances the optical absorption at frequencies corresponding to the excitation energy of a single site. Given the correspondence discussed above between the range  $\omega > 10$  in our example and the visible frequency range, the intermediate region  $\omega \approx 6$  would correspond to the mid-infrared range of frequencies in the cuprates. Indeed, Gao et al [24] report observation of extra optical spectral weight appearing below  $T_c$  in the mid-infrared region.

Table I summarizes the matrix elements for the various optical transitions in the dynamical Hubbard model considered here for the case of a single hole versus the case of two holes on neighboring sites. The weight ratios given in the last column summarize the expected qualitative behavior of spectral weight changes when hole doping increases in the normal state or when the temperature is lowered and the system goes superconducting. We expect the frequency range of the second and third rows to correspond to mid-infrared and that of the fourth row to visible frequencies in the cuprates. Because  $S+1=S > 2S$  for any  $S$ , the optical spectral weight in the mid-infrared range should always increase upon pairing.

## V I. D I S C U S S I O N

We have studied in this paper the behavior of spectral functions in a dynamical Hubbard model by exact diagonalization. The results obtained are exact for the small cluster studied. They support a scenario for the physics of this class of quantum many-body systems that is expected from qualitative arguments and approximate treatments. Namely, that quasiparticles 'undress' in these models when the local hole concentration increases, which occurs both when holes are added to the system (doping) and when holes pair and form Cooper pairs. This scenario is obtained from the exact calculations in this paper without uncontrolled approximations.

The physics of dynamical Hubbard models is especially transparent in the antiadiabatic limit, where the effective Hamiltonian is a Hubbard model with correlated hopping. The results of ref. [13] as well as the results in this paper indicate that the 'intra-band' physics of the model described by the antiadiabatic limit  $\omega_0 \rightarrow 1$  remains essentially unchanged with  $\omega_0$  decreasing to rather small values. In addition to the case  $\omega_0 = 1$  discussed in this paper we also studied the model for  $\omega_0 = 0.5$  and obtained qualitatively similar results. What changes as  $\omega_0$  decreases is that the energy scale of non-intraband excitations decreases up to a point where there is no longer a clear separation between 'intra-band' and 'non-intraband' regions. Nevertheless the low energy physics remains essentially unchanged.

In a more realistic description of a real system there will presumably be a set of excitation energies  $\omega_i$  describing the bosonic excitations that dress the hole quasipar-



ticles. Still we do not expect the physics in such a case to be qualitatively different. These excitations would correspond to local electronic excitations with scale up to eV's. Such energy scales are consistent with experimental observations in cuprates that optical spectral weight in the visible range is transferred to low frequencies both when the system goes superconducting [12] as well as when it is hole-doped in the normal state [25]. Our results in this paper as well as earlier results [26] demonstrate that dynamic Hubbard models naturally describe transfer of spectral weight from high energies unrelated to the scale of superconductivity down to low frequencies when superconductivity sets in, as observed [12,23], hence they provide a natural explanation for the origin of the high energy scale observed in the optical experiments of Moleggraaf et al [12]. The detailed description of such apparently counterintuitive physics remains a challenge for other proposed descriptions of the physics of high temperature superconductors that also propose that superconductivity is driven by kinetic energy lowering [27,28].

The dynamic Hubbard model and the electron-hole symmetric model discussed in this paper are representative of two classes of model Hamiltonians, of which there are many different realizations. In particular, it is not essential that the coupling of the boson in a model in the class of dynamic Hubbard models be to the on-site double occupancy; a model with coupling only to the on-site charge density will also belong to this class if it is not electron-hole symmetric [2]. Also the auxiliary boson may be an oscillator rather than a spin, or the model could have only electronic degrees of freedom [6]. What distinguishes these two classes of models is what is the driving energetics for pairing: in dynamic Hubbard models pairing is kinetic energy driven, and the potential energy increases upon pairing, and the opposite is true in the other class of models, which may be termed 'conventional' or 'electron-hole symmetric'. The conventional electron-phonon models used to describe conventional superconductors belong to this second class of models. We believe that these two classes of models represent very general paradigms. In the class of dynamic Hubbard models the 'undressing' of quasiparticles is essential to lead to kinetic energy lowering; instead, in the 'conventional' class of models the dressing of the quasiparticles may remain unchanged upon pairing if the coupling is weak, or increase in a strong coupling regime.

Dynamic Hubbard models and their low energy effective Hamiltonians can describe superconductivity over the entire range of coupling strengths. The physics is determined by the scale of excitation energies  $\epsilon_0$  and by the strength of the coupling  $g$  or equivalently the magnitude of the 'undressing parameter' (Eq. (28b)). As we have seen in this paper and in ref. [13] the low energy physics is not strongly dependent on the scale  $\epsilon_0$ . The magnitude of  $T_c$  and the superconducting gap is mainly determined by the strength of the dimensionless parameters  $g$  or  $\tilde{g}$  and the single electron hopping parameter  $t$ , as well of course as competing Coulomb repulsions such

as  $U$ . These parameters cannot however be tuned separately at will, in a real system they are all closely interdependent and determined principally by the ionic charge  $Z$  as discussed in refs. [5,6]. For increasing  $g$ ,  $T_c$  becomes large, the coherence length in the superconducting state becomes short and the system becomes incoherent in the normal state for low hole concentration as the magnitude of  $S$  and the quasiparticle weight decrease; the 'undressing' phenomenology becomes particularly apparent in this regime. For small  $g$ ,  $T_c$  becomes small, the coherence length can become thousands of lattice spacings and the normal state becomes coherent; in this regime, even though it is still the same 'undressing physics' that drives the transition to superconductivity, the anomalous spectral weight transfers signaling undressing will become almost invisible. We suggest that it is possible that this same physical mechanism can describe the superconducting phenomenology of materials as distinct as  $\text{YBa}_2\text{Cu}_3\text{O}_{7-x}$ ,  $\text{MgB}_2$ , and  $\text{Al}$  [29].

- 
- [1] J.R. Schrieffer, "Theory of Superconductivity", W. A. Benjamin, New York, 1964.
  - [2] J.E. Hirsch, Phys.Lett. A 134, 451 (1989).
  - [3] J.E. Hirsch and F. Marsiglio, Phys. Rev. B 39, 11515 (1989).
  - [4] J.E. Hirsch, Phys. Rev. B 62, 14487 (2000); 62, 14498 (2000).
  - [5] J.E. Hirsch, Phys. Rev. Lett. 87, 206402 (2001).
  - [6] J.E. Hirsch, Phys. Rev. B 65, 184502 (2002).
  - [7] H. Ding et al, Phys. Rev. Lett. 87, 227001 (2001).
  - [8] Y. Ando et al, Phys. Rev. Lett. 87, 017001 (2001).
  - [9] P.D. Johnson et al, Phys. Rev. Lett. 87, 177007 (2001).
  - [10] D.N. Basov et al, Science 283, 49 (1999).
  - [11] A.F. Santander-Syro et al, cond-mat/0111539 (2001).
  - [12] H.J.A. Moleggraaf, C. Presura, D. van der Marel, P.H. Kes, and M. Li Science 295, 2239 (2002).
  - [13] J.E. Hirsch, cond-mat/0201005 (2002), to be published in Phys. Rev. B.
  - [14] P.M. Aldague, Phys. Rev. B 16, 2437 (1977).
  - [15] J.E. Hirsch, Physica C 199, 305 (1992).
  - [16] J.E. Hirsch and F. Marsiglio, Phys. Rev. B 45, 4807 (1992).
  - [17] J. Wagner, W. Hanke and D.J. Scalapino, Phys. Rev. B 43, 10517 (1991).
  - [18] J.E. Hirsch, Physica C 179, 317 (1991).
  - [19] G.D. Mahan, "Many-Particle Physics" (Plenum, New York, 1981).
  - [20] M. Jarell, Phys. Rev. Lett. 69, 168 (1992).
  - [21] Z.M. Yusof et al, Phys. Rev. Lett. 88, 167006 (2002).
  - [22] F. Marsiglio and J.E. Hirsch, Phys. Rev. B 44, 11960 (1991).
  - [23] I. Fugolet al, Solid St. Comm. 86, 385 (1993).
  - [24] F. Gao, D.B. Romero, D.B. Tanner, J. Talvacchio and M.G. Forrester, Phys. Rev. B 47, 1036 (1993).

- [25] S.Uchida, T.Ido, H.Takagi, T.Arima, Y.Tokura and S.Tajima, Phys.Rev.B 43, 7942 (1991).  
 [26] J.E.Hirsch, Physica C 201, 347 (1992).  
 [27] E.W.Carlson, D.Orgad, S.A.Kivelson and V.J.Emery, Phys.Rev.B 62, 3422 (2000).  
 [28] P.W.Anderson, Physica C 341-348, 9 (2000).  
 [29] J.E.Hirsch, cond-mat/0106310 (2001), to be published in "Studies of High Temperature Superconductors", Vol. 38, ed.by A.Narlikar, Nova Sci.Pub., New York.

FIG. 1. Effective interaction Eq. (21) versus on-site repulsion  $U$  for the dynamical Hubbard model with  $g = 3$  and  $\beta_0 = 1$  (full line) and in the antiadiabatic limit  $\beta_0 = 1$  (dashed line). The same parameters ( $g = 3; \beta_0 = 1$ ) are used in the following figures.

FIG. 2. Energy levels for the dynamical Hubbard model. The energy levels for a single hole in the four-site cluster and for two holes with on-site repulsion  $U = 8$  and  $U = 0$  are shown.

FIG. 3. Frequency-dependent conductivity for dynamical Hubbard model with two holes and on-site repulsion  $U = 8$  and  $U = 0$ . The  $\chi$ -functions in Eq. (8) are broadened to Lorentzians with width  $\gamma = 0.5$ . The lowest frequency function at frequency  $\beta_0$  ('Dude precursor') is shifted to  $\beta = 0$  and represented by a Dude form (semi-Lorentzian) with width  $\gamma = 0.5$ .

FIG. 4. (a) Kinetic energies for dynamical Hubbard model versus on-site  $U$ , obtained from integration of  $\chi_1(\beta)$  from Eqs. (12) and (16). The cutoff frequency to define the 'intra-band' spectral weight  $A_1$  is  $\beta_m = 2$ . The dash-dotted line gives the results for twice the total optical spectral weight  $A_1 + A_H$  for a single hole in the cluster, which coincides with the results for two holes in the cluster for large  $U$ . The dotted line gives twice the intra-band optical spectral weight for one hole, which is approximately equal to the intra-band spectral weight for two holes in the cluster for large  $U$ . The intra-band spectral weights for two holes are shown both for  $\beta_0 = 1$  and in the antiadiabatic limit  $\beta_0 = 1$ ; for one hole in the antiadiabatic limit the results are indistinguishable from the value for  $\beta_0 = 1$ . (b) Ratio of intra-band to inter-band optical spectral weight versus  $U$  for  $\beta_0 = 1$ .

FIG. 5. One-particle spectral function for hole destruction in the system with one hole (a) and with two holes (b). The functions are broadened to Lorentzians with width  $\gamma = 0.1$ . The spectral weight at frequencies above  $\beta = 10$  is very small and is amplified in the figure by a factor 50.

FIG. 6. Same as figure 5 for hole creation in the system with zero holes (a) and with one hole (b).

FIG. 7. Quasiparticle weights versus  $U$  for the system with two holes (dashed line) and with one hole (full line). The corresponding quasiparticle weights in the antiadiabatic limit are shown as the dash-dotted and dotted lines respectively.

FIG. 8. Effective interaction Eq. (21) versus on-site repulsion  $U$  for the electron-hole symmetric model Eq. (5), with  $g = 3$  and  $\beta_0 = 1$  (full line) and in the antiadiabatic limit  $\beta_0 = 1$  (dashed line). The same parameters ( $g = 3; \beta_0 = 1$ ) are used in the following figures.

FIG. 9. Frequency-dependent conductivity for the electron-hole symmetric model with two holes and on-site repulsion  $U = 2$  and  $U = 0$ .

FIG. 10. (a) Kinetic energies for electron-hole symmetric model versus on-site  $U$ . The cutoff frequency to define the 'intra-band' spectral weight  $A_1$  is  $\beta_m = 2$ . The dash-dotted line gives the results for twice the total optical spectral weight  $A_1 + A_H$  for a single hole in the cluster, and the dotted line gives the corresponding intra-band value. (b) Ratio of intra-band to inter-band optical spectral weight versus  $U$ .

FIG. 11. One-particle spectral function for hole destruction in the electron-hole symmetric model with one hole (a) and with two holes (b).

FIG. 12. Same as figure 11 for hole creation in the system with zero holes (a) and with one hole (b).

FIG. 13. Quasiparticle weights versus  $U$  for the electron-hole symmetric model with two holes (dashed line) and with one hole (full line). The corresponding quasiparticle weights in the antiadiabatic limit are shown as the dash-dotted and dotted lines respectively.

FIG. 14. (a) Ratio of effective mass of a single hole to the effective mass of a hole in a pair, calculated from the ratio of intra-band kinetic energies, versus effective interaction  $U_{eff}$  (Eq. (21)) for both models. For the dynamical Hubbard model this ratio increases as  $U_{eff}$  decreases and the pair forms, while for the electron-hole symmetric model it decreases. (b) Ratio of quasiparticle weights of a hole in the system with two holes to the quasiparticle weight of the single hole, versus effective interaction. In the dynamical Hubbard model this ratio increases as  $U_{eff}$  decreases and the pair forms, in the electron-hole symmetric model it decreases.

FIG. 15. Optical conductivity of the dynamic Hubbard model for two holes and on-site repulsion  $U = 0$  for various temperatures (in units of the bare hopping  $t$ ). Note the transfer of spectral weight from high frequencies ( $\omega > 10$ ) to low frequencies as the temperature is lowered.

TABLE I. Optical transitions, possible states of auxiliary spin. The ground state and excited state of the auxiliary spin at a site with  $n$  holes are denoted by  $|j\rangle$  and  $|j^*\rangle$  respectively. The four left columns correspond to transitions involving a single hole hopping between neighboring sites,  $|j\rangle \rightarrow |j^*\rangle$ ; the four right columns correspond to transitions involving two holes at neighboring sites,  $|j\rangle \rightarrow |j^*\rangle$ .

initial state	nal state	weight	energy	initial state	nal state	weight	energy	weight ratio
$ j\rangle \rightarrow  j^*\rangle$	$ j\rangle \rightarrow  j^*\rangle$			$ j\rangle \rightarrow  j^*\rangle$	$ j\rangle \rightarrow  j^*\rangle$			
$ j\rangle \rightarrow  j^*\rangle$	$ j\rangle \rightarrow  j^*\rangle$	$S^2$	intra-band	$ j\rangle \rightarrow  j^*\rangle$	$ j\rangle \rightarrow  j^*\rangle$	$S$	intra-band	$1/S > 1$
	$ j\rangle \rightarrow  j^*\rangle$	$S$	$\frac{1}{2} \frac{1+g^2}{1+g^2}$		$ j\rangle \rightarrow  j^*\rangle$	$1$	$\frac{1}{2} \frac{1+g^2}{1+g^2}$	$1/S > 1$
	$ j\rangle \rightarrow  j^*\rangle$	$S$	$\frac{1}{2} \frac{1+g^2}{1+g^2}$		$ j\rangle \rightarrow  j^*\rangle$	$S^2$	$\frac{1}{2} \frac{1+g^2}{1+g^2}$	$S < 1$
	$ j\rangle \rightarrow  j^*\rangle$	$1$	$\frac{1}{2} \frac{1+g^2}{1+g^2}$		$ j\rangle \rightarrow  j^*\rangle$	$S$	$\frac{1}{2} \frac{1+g^2}{1+g^2}$	$S < 1$

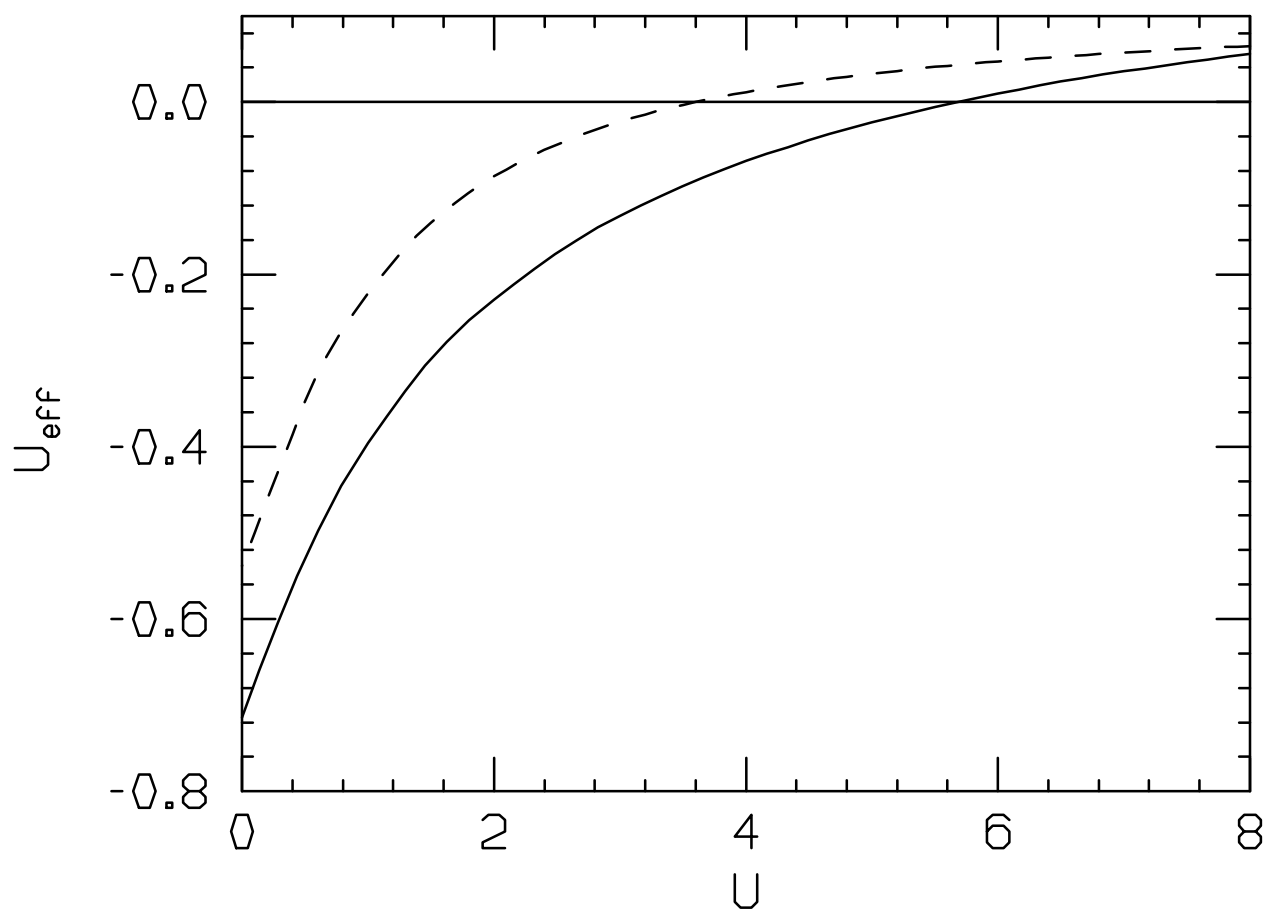


Figure 1

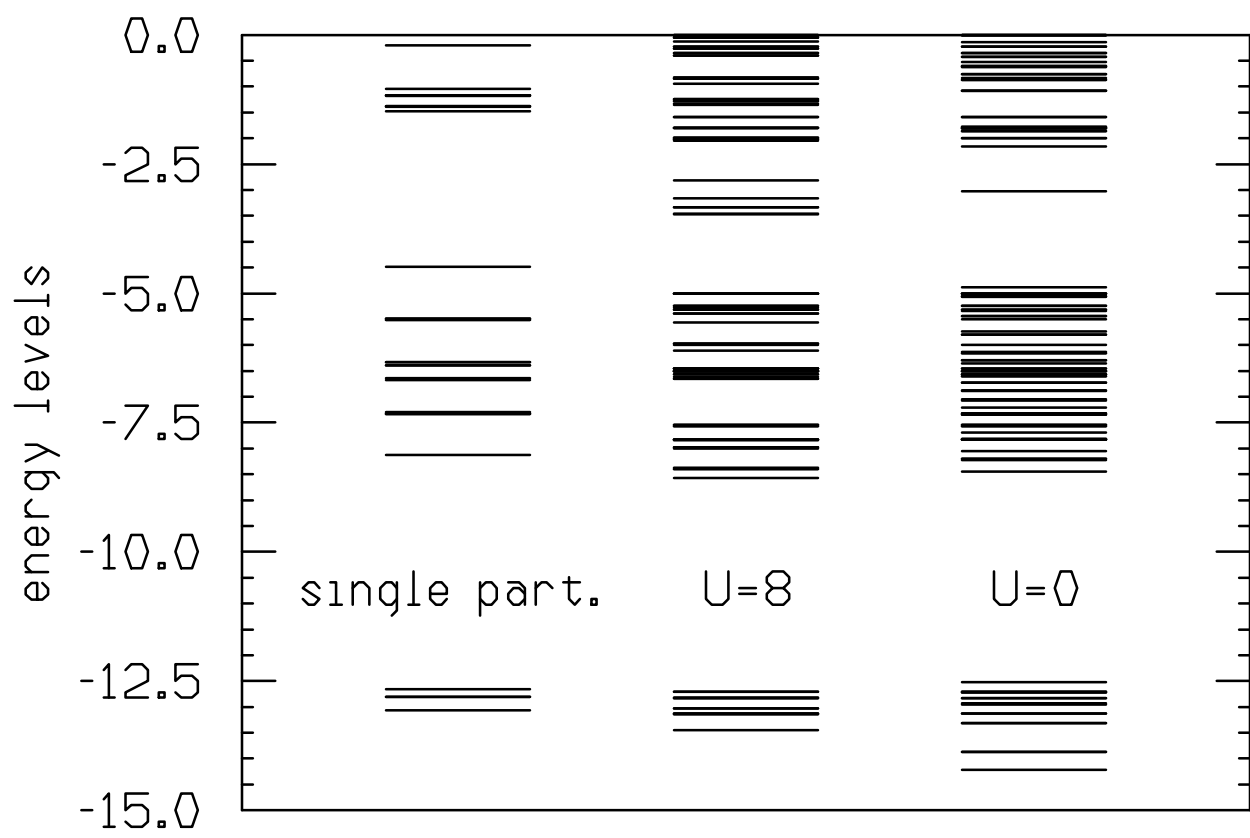


Figure 2

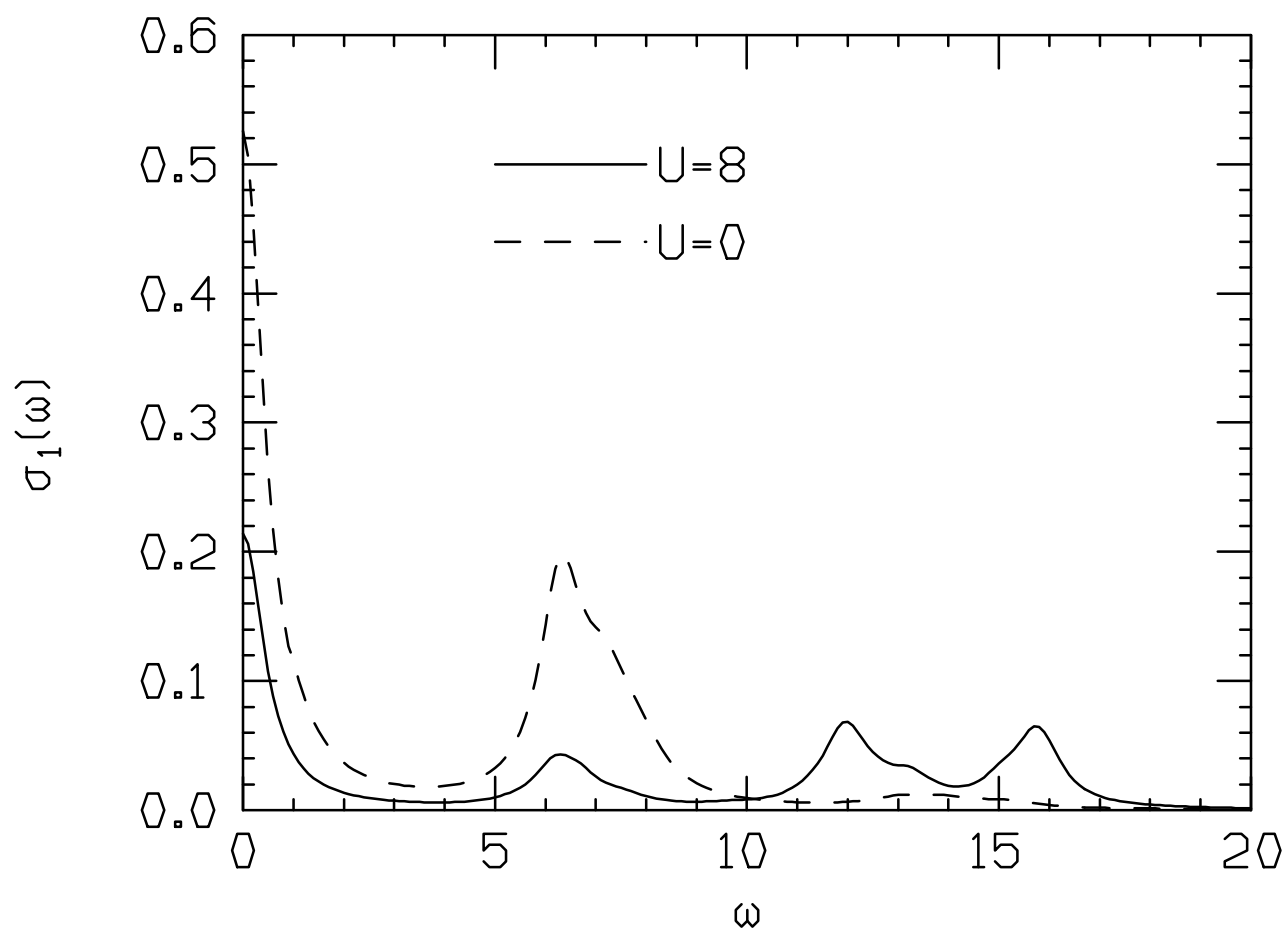


Figure 3

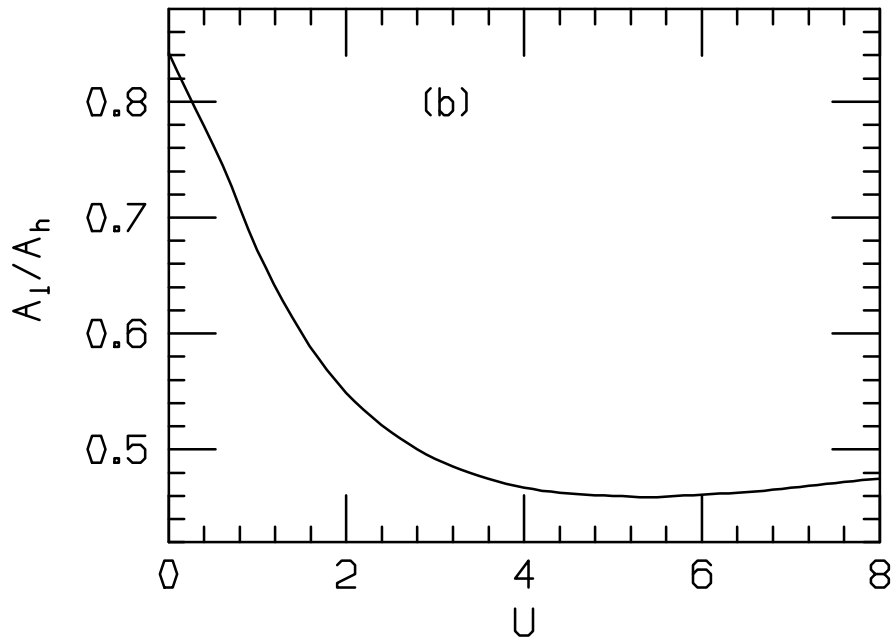
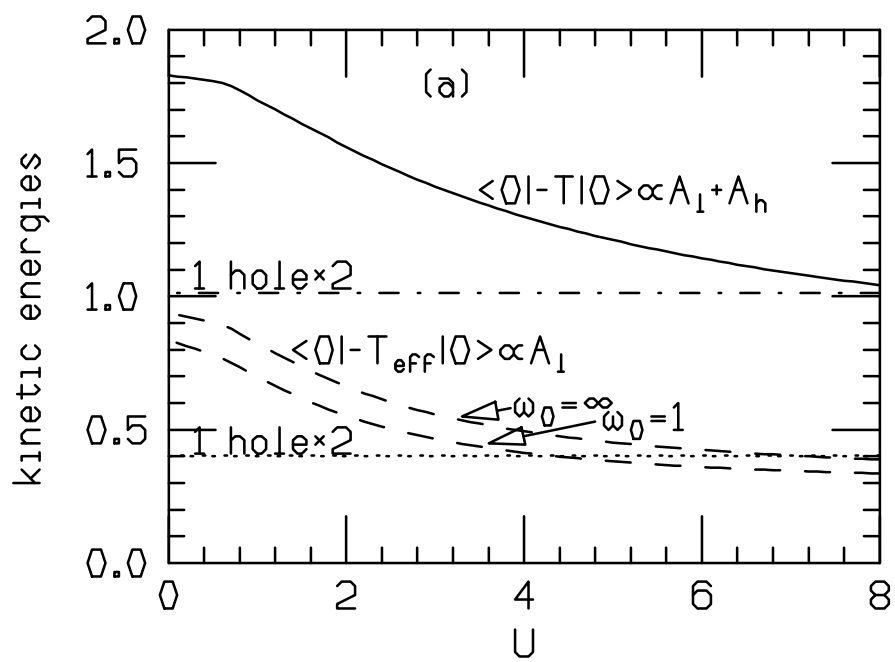


Figure 4

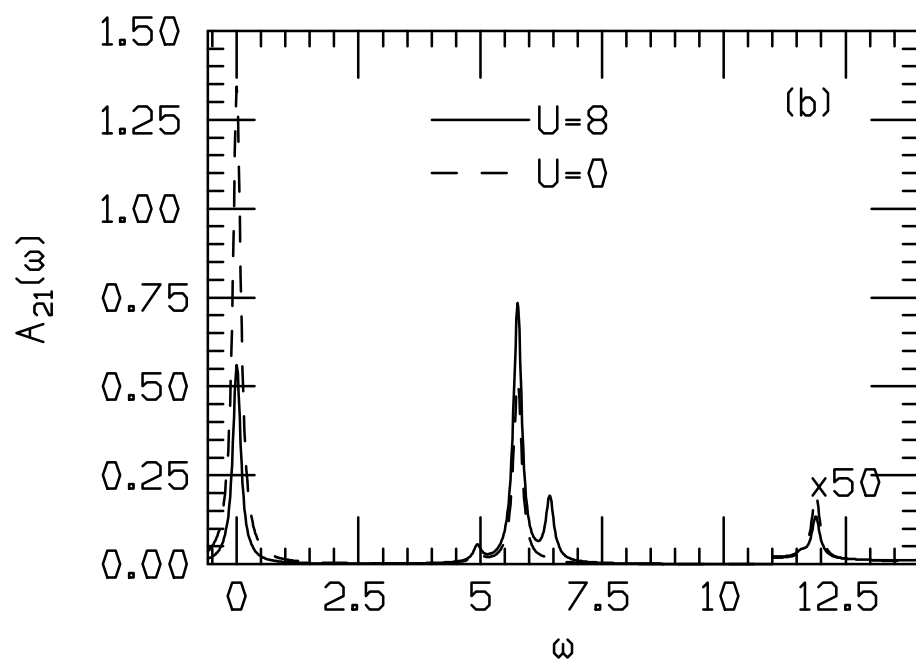
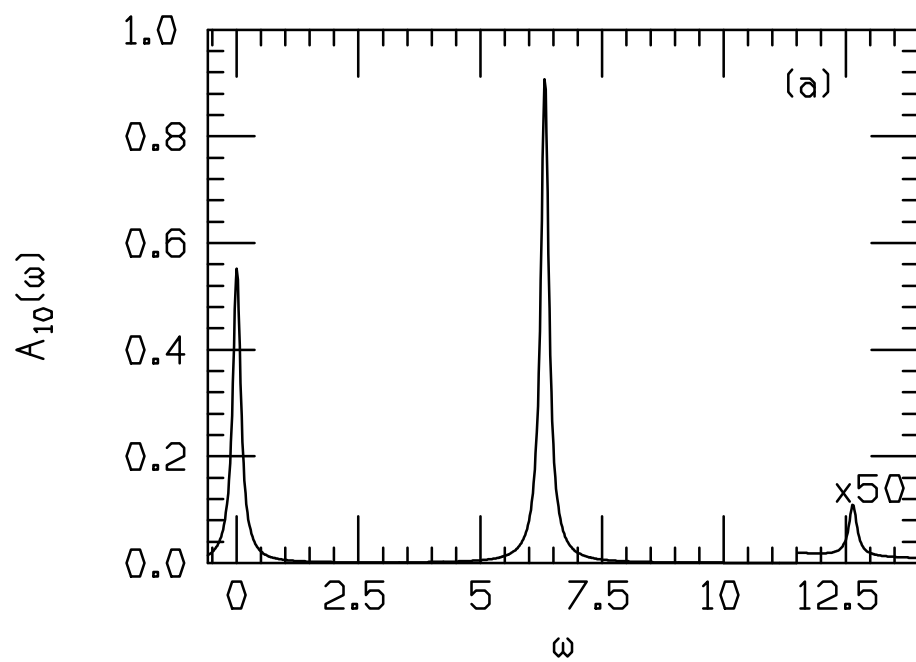


Figure 5



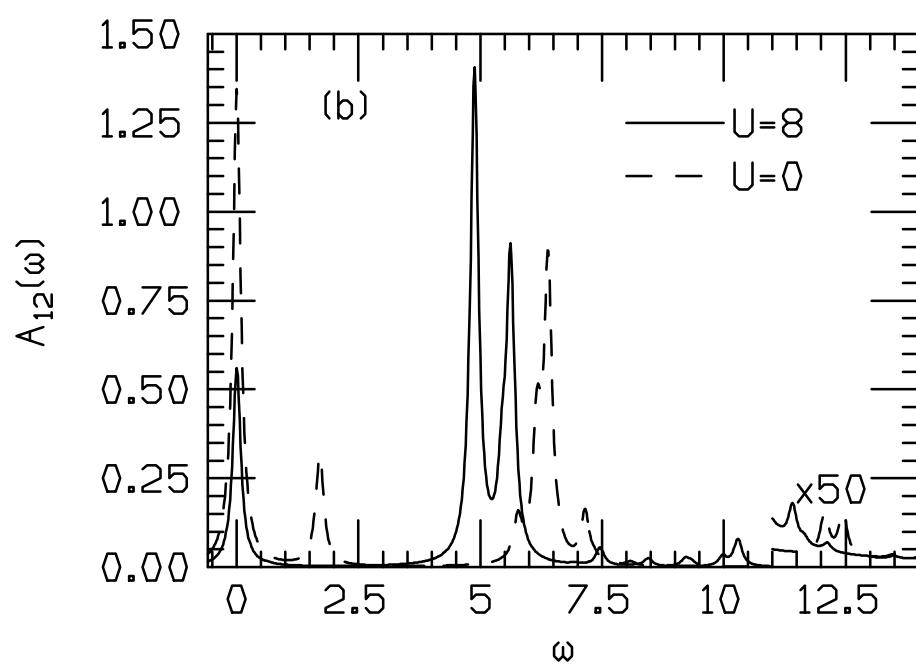
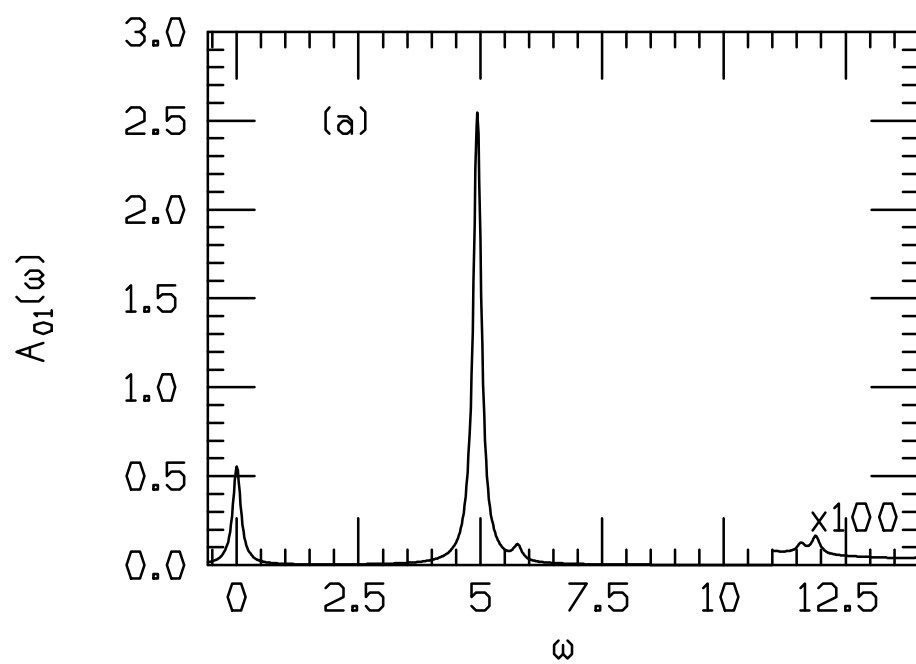


Figure 6

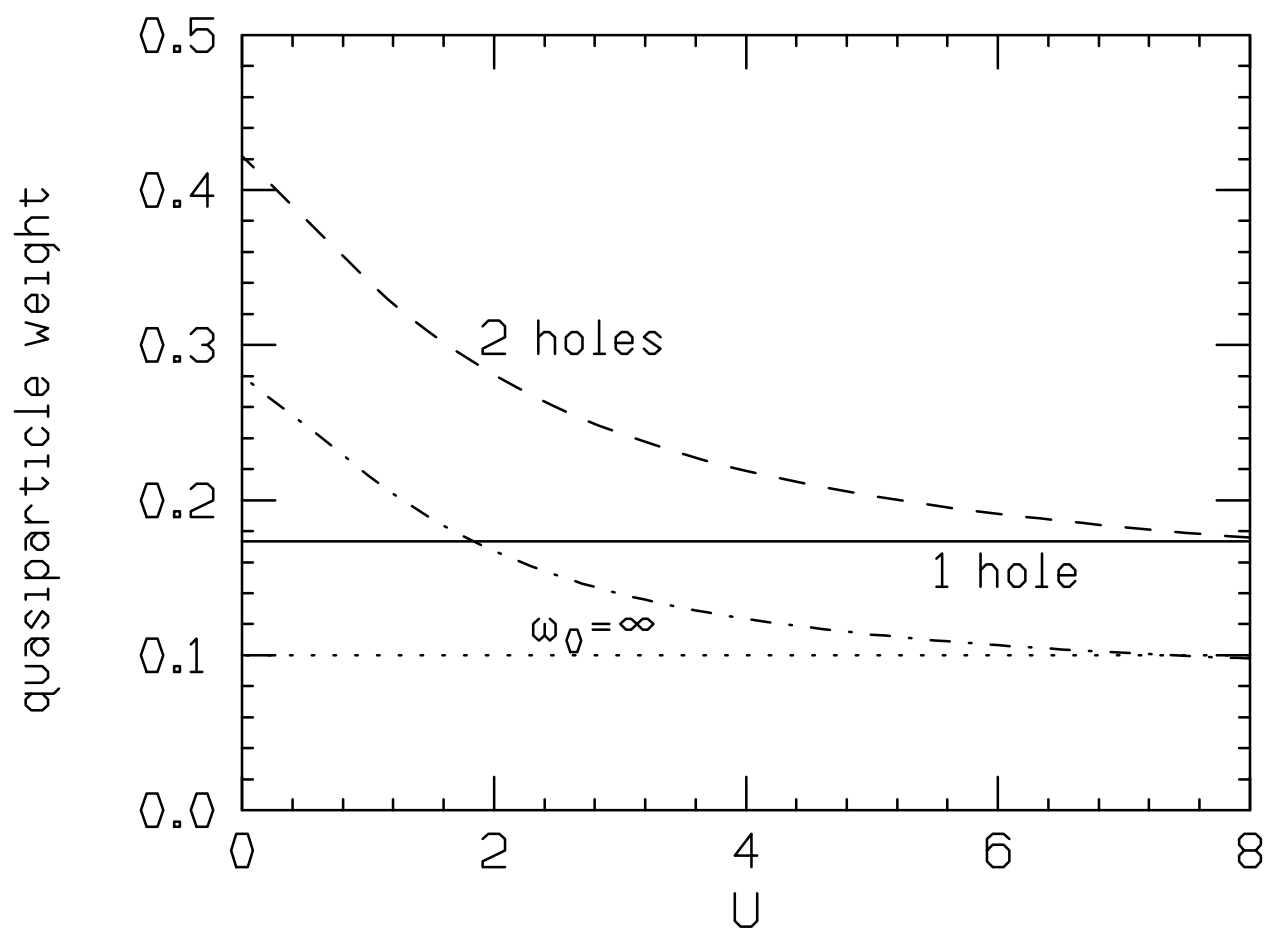


Figure 7

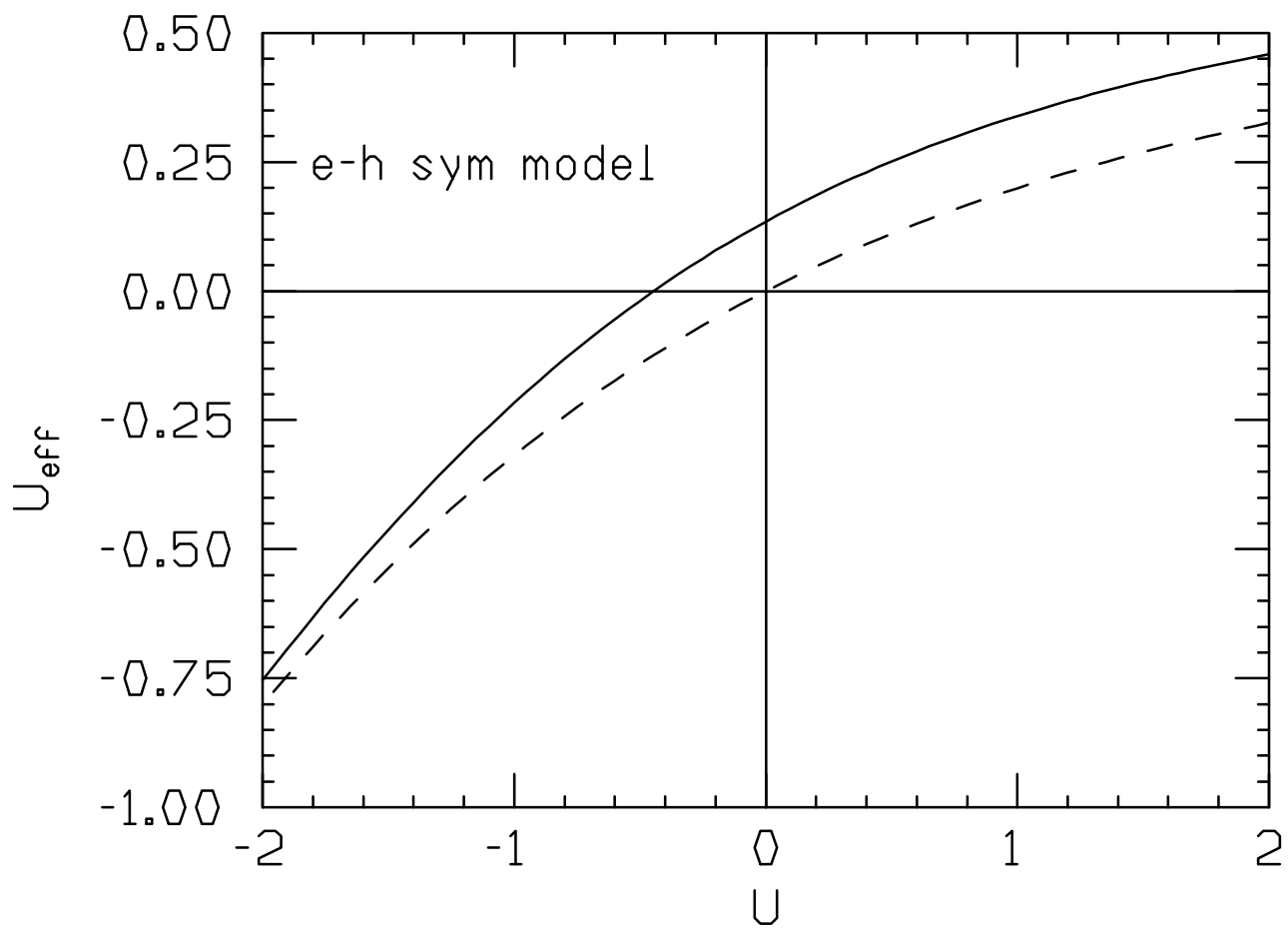


Figure 8

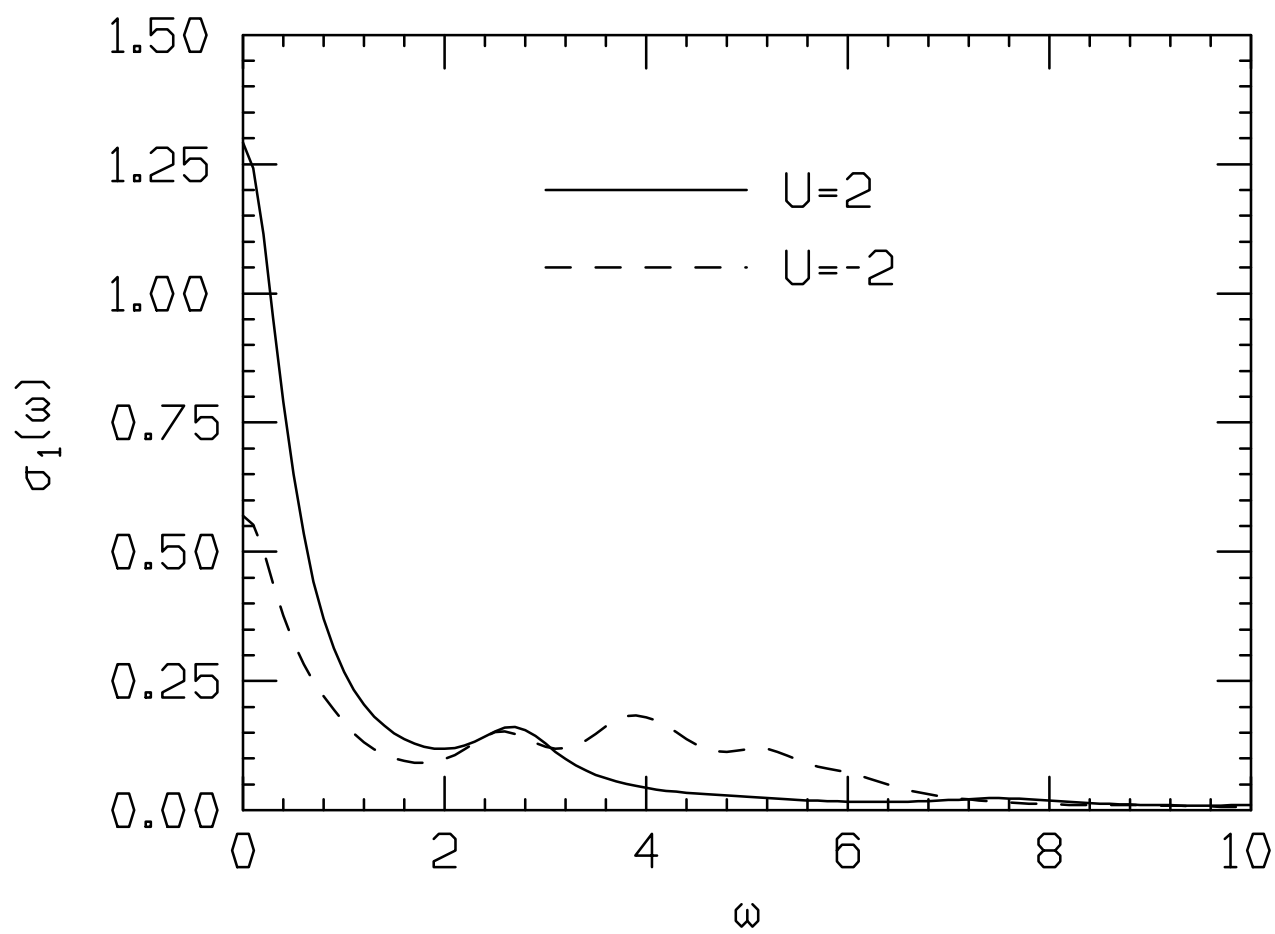


Figure 9

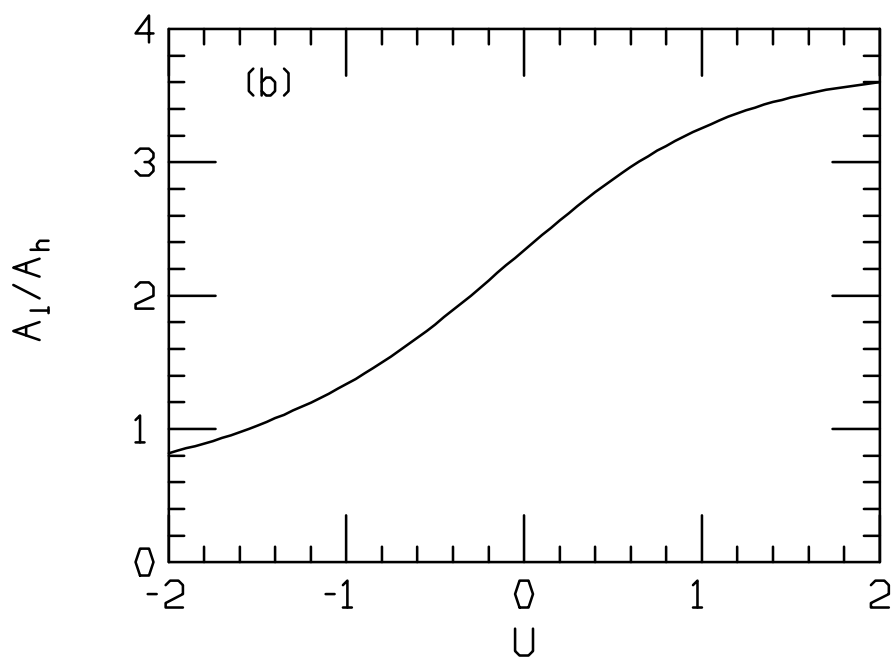
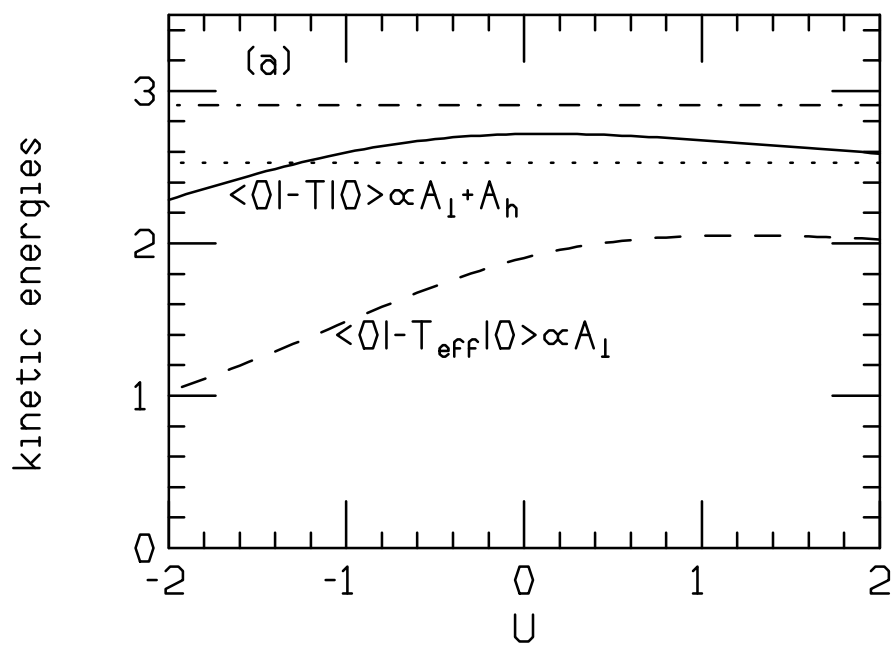


Figure 10

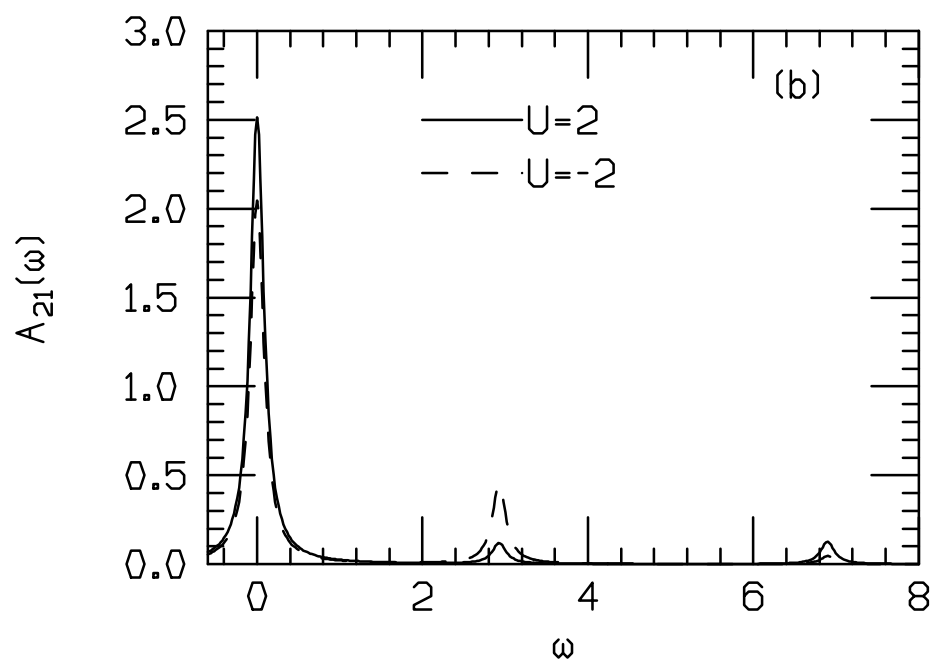
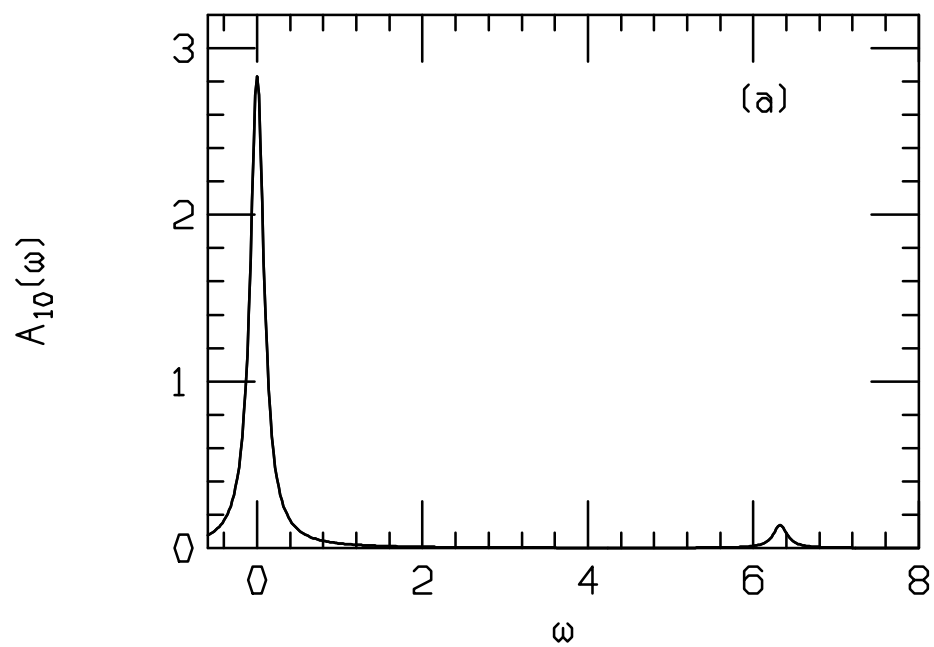


Figure 11

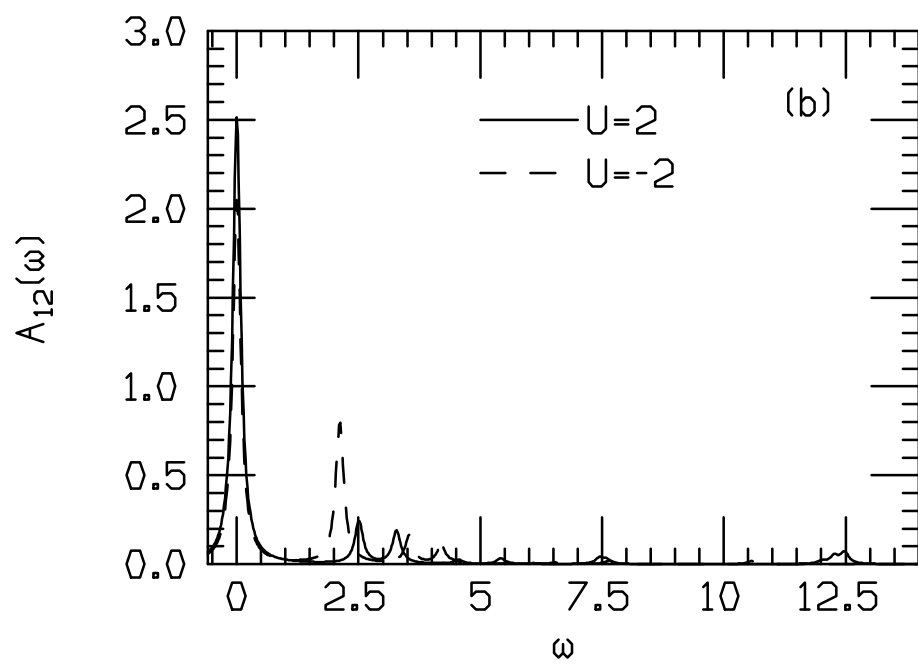
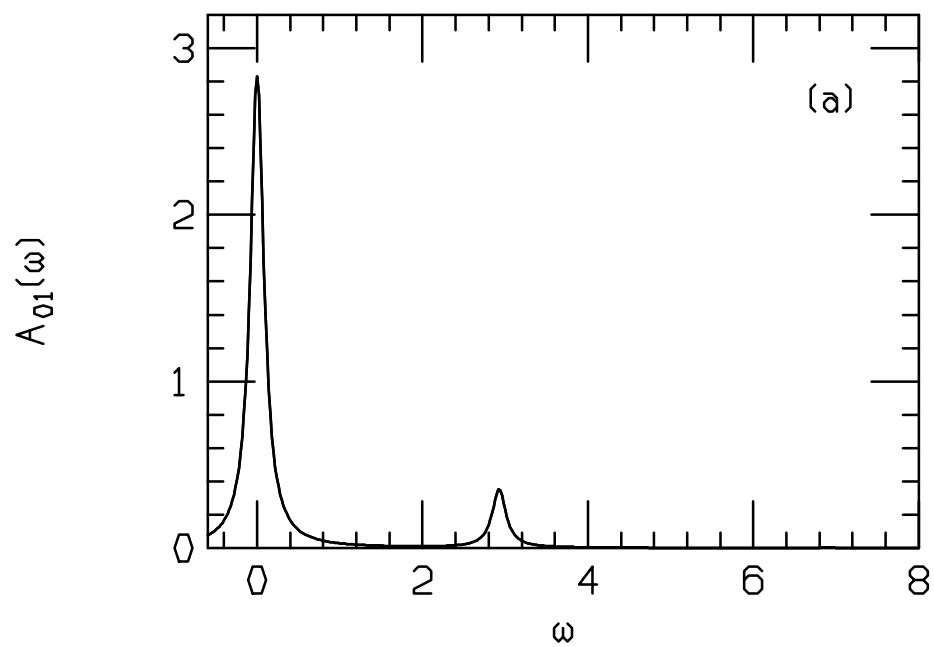


Figure 12

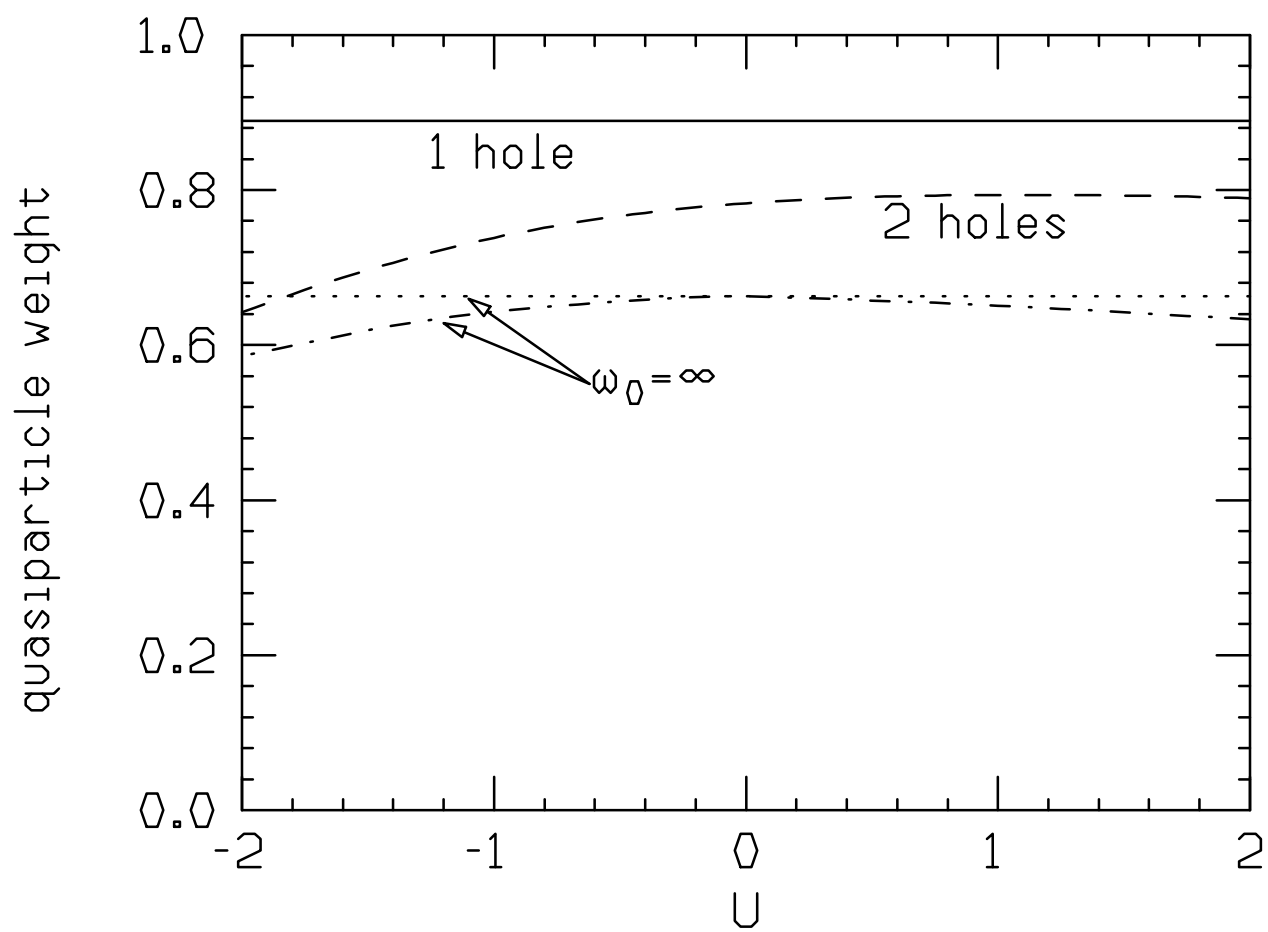


Figure 13



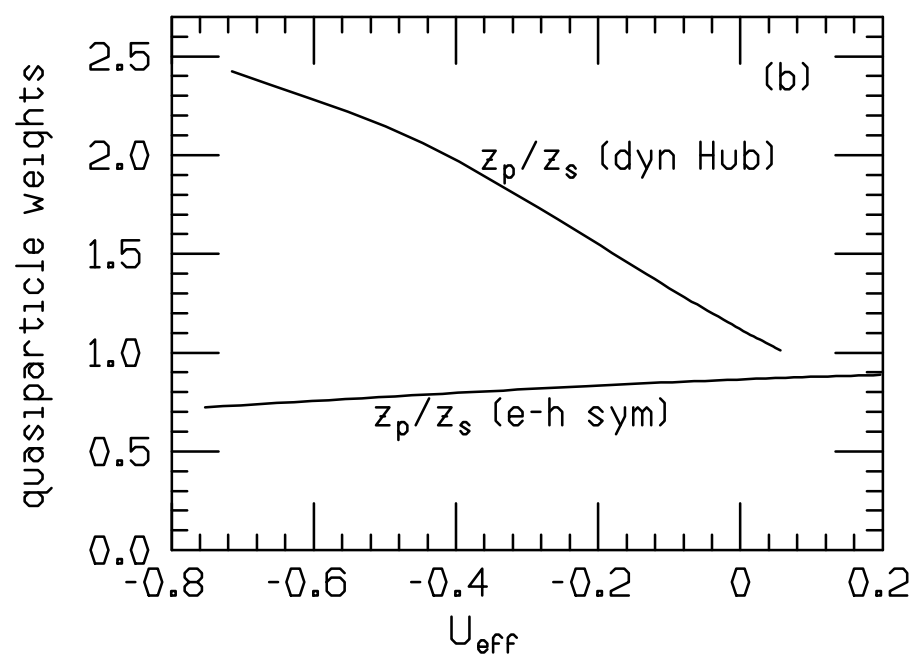
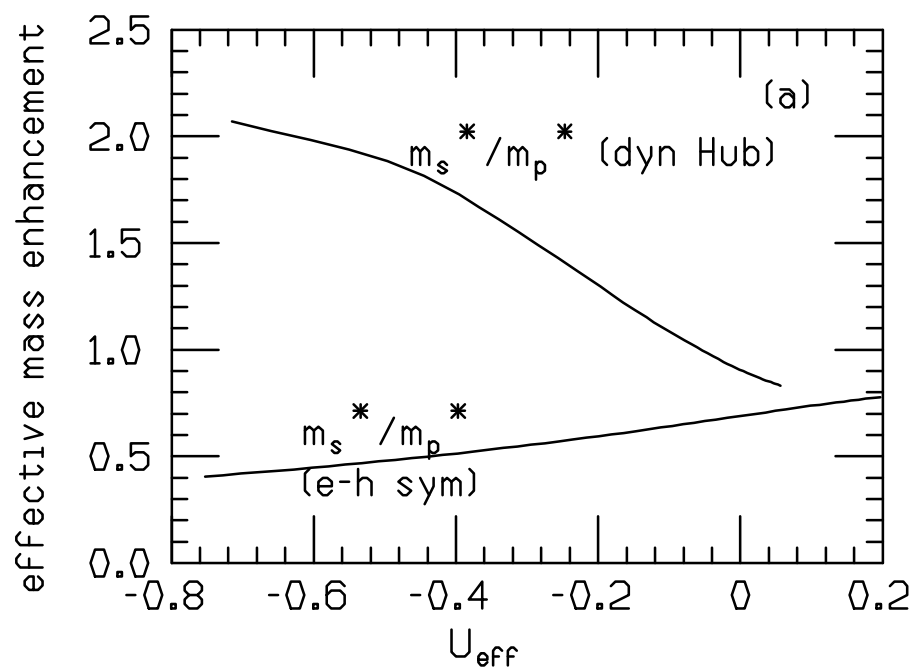


Figure 14

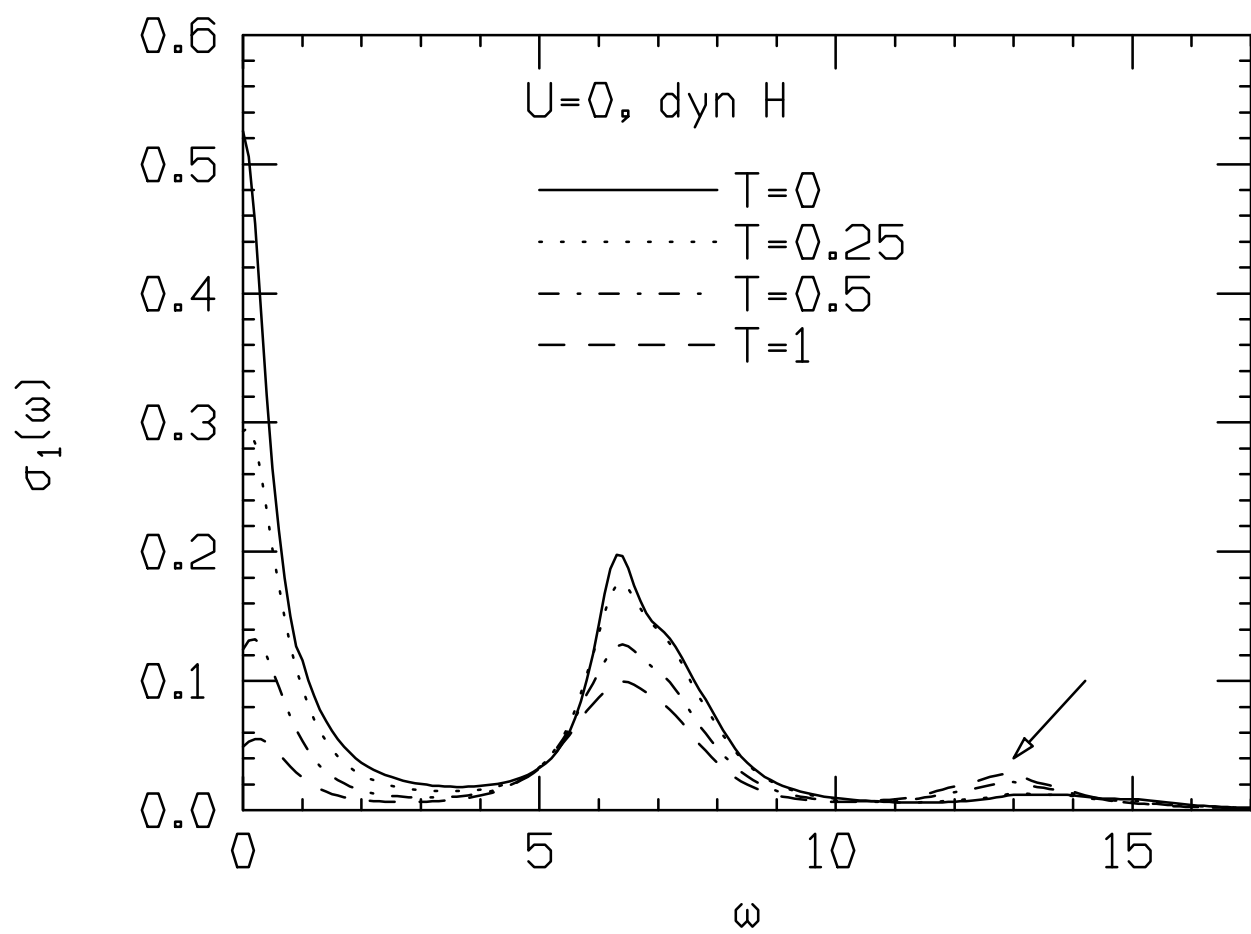


Figure 15